J. Mar. Sci. Eng. **2015**, *3*, 560-590; doi:10.3390/jmse3030560

OPEN ACCESS

Journal of
Marine Science and Engineering
ISSN 2077-1312
www.mdpi.com/journal/jmse

Article

Coastal Flood Assessment Based on Field Debris Measurements and Wave Runup Empirical Model

David Didier *, Pascal Bernatchez, Geneviève Boucher-Brossard, Adrien Lambert, Christian Fraser, Robert L. Barnett and Stefanie Van-Wierts

Coastal Geoscience, Centre for Northern Studies, University of Quebec in Rimouski, Rimouski, QC G5L3A1, Canada

* Author to whom correspondence should be addressed; E-Mail: David_Didier@uqar.ca; Tel.: +1-418-723-1986 (ext. 1364).

Academic Editor: Rick Luettich

Received: 22 April 2015 / Accepted: 23 June 2015 / Published: 15 July 2015

Abstract: On 6 December 2010, an extra-tropical storm reached Atlantic Canada, causing coastal flooding due to high water levels being driven toward the north shore of Chaleur Bay. The extent of flooding was identified in the field along the coastline at Maria using DGPS. Using the assumption that the maximum elevation of flooded areas represents the combination of astronomical tide, storm surge and wave runup, which is the maximum elevation reached by the breaking waves on the beach, all flood limits were identified. A flood-zone delineation was performed using GIS and LiDAR data. An empirical formula was used to estimate runup elevation during the flood event. A coastal flood map of the 6 December flood event was made using empirical data and runup calculations according to offshore wave climate simulations. Along the natural beach, results show that estimating runup based on offshore wave data and upper foreshore beach slope represents well the observed flood extent. Where a seawall occupies the beach, wave breaking occurs at the toe of the structure and wave height needs to be considered independently of runup. In both cases (artificial and natural), flood risk is underestimated if storm surge height alone is considered. There is a need to incorporate wave characteristics in order to adequately model potential flood extent. A coastal flooding projection is proposed for Pointe Verte based on total water levels estimated according to wave climate simulation return periods and relative sea-level rise for the Chaleur Bay.

Keywords: storm surge; wave runup; coastal flood mapping; coastal defense

1. Introduction

Sea-level rise, as a consequence of climate change, is a primary concern to coastal communities due to the increased threat of storm surges and coastal flooding [1,2]. The rate of global mean sea-level rise increased from 1.9 mm/year to 3.2 mm/year between the periods 1961 to 2009 and 1993 to 2011 [3,4]. This acceleration, combined with future projections of sea level and extreme water level change [5–11] has led the scientific community to pay greater attention to the development of vulnerability assessment methods for coastal communities and infrastructure to flooding phenomenon [12]. Previously, the vulnerability of coastal communities to future sea-level rise has been estimated by applying hypothetical sea-level increases (e.g. often a hypothetical 1 m rise is used, [13–15]) or predictions from SRES and IPCC scenarios [16,17] to topographic maps or digital elevation models at national or greater scales [18,19]. However, adaptation approaches to coastal flooding require the development of local to regional level assessments [20]. In this context, the regional distribution and amplitude of sea-level rise remains a significant uncertainty when forecasting future trends [6]. In addition, the isostatic component (vertical land motion) is still rarely accounted for in coastal flooding assessment methods. It is evidently essential, therefore, to assess future *relative* sea-level rise [21], especially in areas experiencing crustal subsidence due to postglacial isostasy [22,23].

Coastal flooding occurs when water levels overtop the first natural ridge or flood defense crest landward of the beach, generating landward flow and sediment transport [24]. Alongshore water level variability, relative to the crest elevation, further affects overwash potential [25] and can lead to an increase in the risk of flooding. During coastal storms, resulting water level maxima are a product of astronomical tide, barometric pressure and wind-induced surge [26,27]. In addition, landward propagating waves in shallow waters are affected by beach morphology due to the effects of, e.g., shoaling, wave breaking and energy dissipation [28]. Such interactions can increase water levels in the onshore direction through the process of wave runup following breaking in the surf zone [29]. Runup (R) is defined as the vertical elevation difference between the maximum shoreward location of water and still water level (predicted tide + surge) [30–32] and includes two components: the setup and swash [33]. Setup is defined as a mean water surface elevation in response to wave breaking, which is a superelevation, whereas swash refers to oscillations across the water-land interface around setup. The sum of tide prediction (T_{pred}), surge (S_{surge}) and runup on natural beaches correspond to total water levels (TWL) [34,35]. Runup is generally calculated in terms of the two percent exceedance value of wave runup ($R_{2\%}$) for the TWL [34].

Runup (R) on a natural beach mainly depends on offshore significant wave height (H_0) and wavelength ($L_0 = gT^2/2\pi$; where g is the acceleration due to gravity (981m/s), T is the wave period (s)) and the beach slope [29,36–38] grouped under the non-dimensional Iribarren number ξ. The Iribarren number, also referred to surf zone similarity parameter, is widely used in the computation of runup and overtopping discharge [37] and in near-shore process assessments [28]. Beach slope is therefore an important parameter for determining maximum wave runup height along coasts. However,

beach surfaces used to calculate slopes, which can differ significantly between case studies, are not always clearly identified or described in the literature [29,32,34,39].

Wave runup on structures is typically calculated using a design wave for an expected water level in order to determine the required crest elevation for defense structures [40]. Types of structures range from low sloping coastal defenses to vertical seawalls. The main factors that influence flooding over sloping structures are wave runup and overtopping [41,42]. However, for vertical seawalls where $\xi = \infty$, wave runup is minimal and is limited to a theoretical value of $R_{2\%}/H_0 = 1.4$ [43]. In such cases, where waves frequently impact the structure, wave height is usually twice the incident wave amplitude and can produce a vertical plume of *circa* 5.5 times the wave amplitude [44]. On sloping coastal defenses, such as dykes, wave overtopping occurs when wave runup exceeds the height of defense structures [45].

It is a challenge to accurately model the landward flow of water following overtopping of defense structures due to complex interactions between wave morphology and the structures themselves [46]. Studies on flow characteristics and discharge rates following wave overtopping have highlighted the importance of the roughness factor and permeability associated with different defense structures [47,48]. Whereas overtopping associated with different coastal structure types has been evaluated [47,49], less is known on the spatial propagation of water levels in backshore zones following overtopping of the structures [46], which is of key relevance to coastal managers responsible for land use planning and flood risk management [50]. Moreover, the establishment of rigid defense structures in response to ongoing erosion processes often results in decreasing beach and intertidal zone widths [51]. This can lead to increased wave overtopping of defense structures during storms [52,53]. Such modifications to natural beach states can increase flood risk [51,54]. The alongshore variability in flood elevation as a result of human intervention in response to coastal hazard represents a threat to coastal communities.

Studies on runup have typically been carried out along stretches of natural beaches (e.g. [29,38,55–57]] or in areas of armoured coastline (e.g. [41,42]). In reality, coastal zones prone to flood risk will contain a combination of both natural and artificial sections, which highlights the need for a local to regional approach when considering coastal flooding vulnerability.

To date, the majority of coastal flooding studies have been carried out along coastlines exposed to ocean swell with long fetch and rarely on sheltered embayments [58]. In sheltered coastal environments, it is generally considered that the waves have less influence on coastal flooding and the tide and storm surge are the main drivers [58]. In Eastern Canada, the entire area of the Chaleur Bay (Figure 1) has been hit by two major and destructive storms recorded within a five year interval (December 2005 to December 2010), despite the fact that the Acadian peninsula partially protect the bay to wave agitation coming from the Gulf of St. Lawrence. However, the recent storm events have raised questions with regards to the influence of wave effects along coastlines in sheltered bays with short fetch. There is a critical need to understand wave influence in these environments in order to adapt and improve coastal zone management in Eastern Canada.

Mapping coastal flood risk areas is an important step for risk management planning and for guiding adaptation procedures necessary to reduce vulnerability to flooding. The classical method of flood mapping, which typically integrates extreme water levels, derived from historic tide gauge data, with a digital elevation model ("bathtub model") to identify areas at risk [31,59–61], has been criticized in recent years [62]. Recent storm events along North American (e.g. Katrina, Wilma, Sandy) and European (e.g. Xynthia) coastlines have highlighted the need to understand the effects of beach geomorphology

and hydrodynamic conditions close to the coast in order to accurately determine backshore zones at risk of flooding [20,31,34]. Due to a paucity of wave data at local to regional scales, wave runup is not always included in coastal flood mapping. This is especially prevalent in Atlantic Canada [63,64]. Another challenge to flood risk mapping derives from forecasting extreme water level return periods based only on short tide gauge series [65,66]. It is also important to integrate the probability of extreme tidal water levels with runup data [34] for future coastal management and robust flood hazard mapping. Recent studies have shown that airborne LiDAR data, widely used for digital elevation models in flood hazard mapping, are not precise enough to accurately identify crest elevations of the first line of defense and to represent adequately elevation changes of flood defenses (embankment crests and walls) or beach berms at the coastal front or along river banks, which leads to over- or under-estimating of risk areas [67–70].

The development of methods for flood hazard mapping remains a challenge, especially at the local to regional scale, in order to be applicable and easy to use by local authorities responsible for land use and risk management. Therefore, only few approaches integrate the different components required to effectively map the exposed areas to flood hazards for the future.

The aim of this paper is to develop a coastal flood mapping approach based on *in situ* measurements, modelled wave characteristics, sea-level rise, estimated extreme water levels return periods, and wave runup estimations using empirical formula. This method is compared and validated from field surveys during and immediately after the 6 December 2010 storm event that caused extensive damage to the coast of Eastern Canada. We compare the altitude reached by the total water level during the storm based on the presence or not of coastal defenses and assess the importance of the waves in the flood pattern for sheltered coasts. Since slope determination is often of primary concern in runup parameterization, a focus was made on beach morphology with a mobile terrestrial LiDAR system (MTLS) to calculate beach slopes. The use of terrestrial LiDAR system also aims to solve the problem of identifying the elevation crest of the first coastal defense line. Finally, the proposed approach addresses future coastal flood scenarios at the community scale that can be easy to apply for coastal managers.

2. Study Area

In Atlantic Canada, common extra-tropical cyclones typically generate northwestern and northeastern winds toward the shores of the Gulf of St. Lawrence, creating storm surges and high waves [71,72]. As a result of these low-pressure systems, coastal flooding and erosion have increased in recent years throughout the Chaleur Bay [73]. The study area is located in the municipality of Maria (Figure 1) on the north shore of the Chaleur Bay in the province of Quebec, Eastern Canada. Maria represents a typical coastal community for Eastern Canada, with a population of 2500 and an established mix of infrastructure (such as residential, recreational, commercial and tourism). The national road, 132, which links coastal towns throughout the Gaspé Peninsula with eastern Quebec, is particularly vulnerable to flooding at Maria [74]. Despite damage caused by several flooding events [75], there is currently no coastal flood hazard mapping in the province of Quebec.

Flood hazard has been assessed for the southeast part of Maria where there are more than 40 houses built on the sandy low-lying coast (Figure 1). This area was flooded both on 2 December 2005 and 6 December 2010. This stretch of coastline contains a uniform sandy and gravel beach to the east (~22 m width), which is in a quasi-natural state (Figure 2a) and a protected zone to the west, which

contains a wooden seawall protecting different properties [52]. The eastern section contains some low lying coastal defenses, which are situated landward of the beach or on the upper beach, with a structure toe above HAT. We therefore assume an alongshore and natural wave energy dissipation across the beach in this area, where runup can occur on the sloping beach, as underlined by the Mase *et al*. [41] study on wave runup and overtopping.

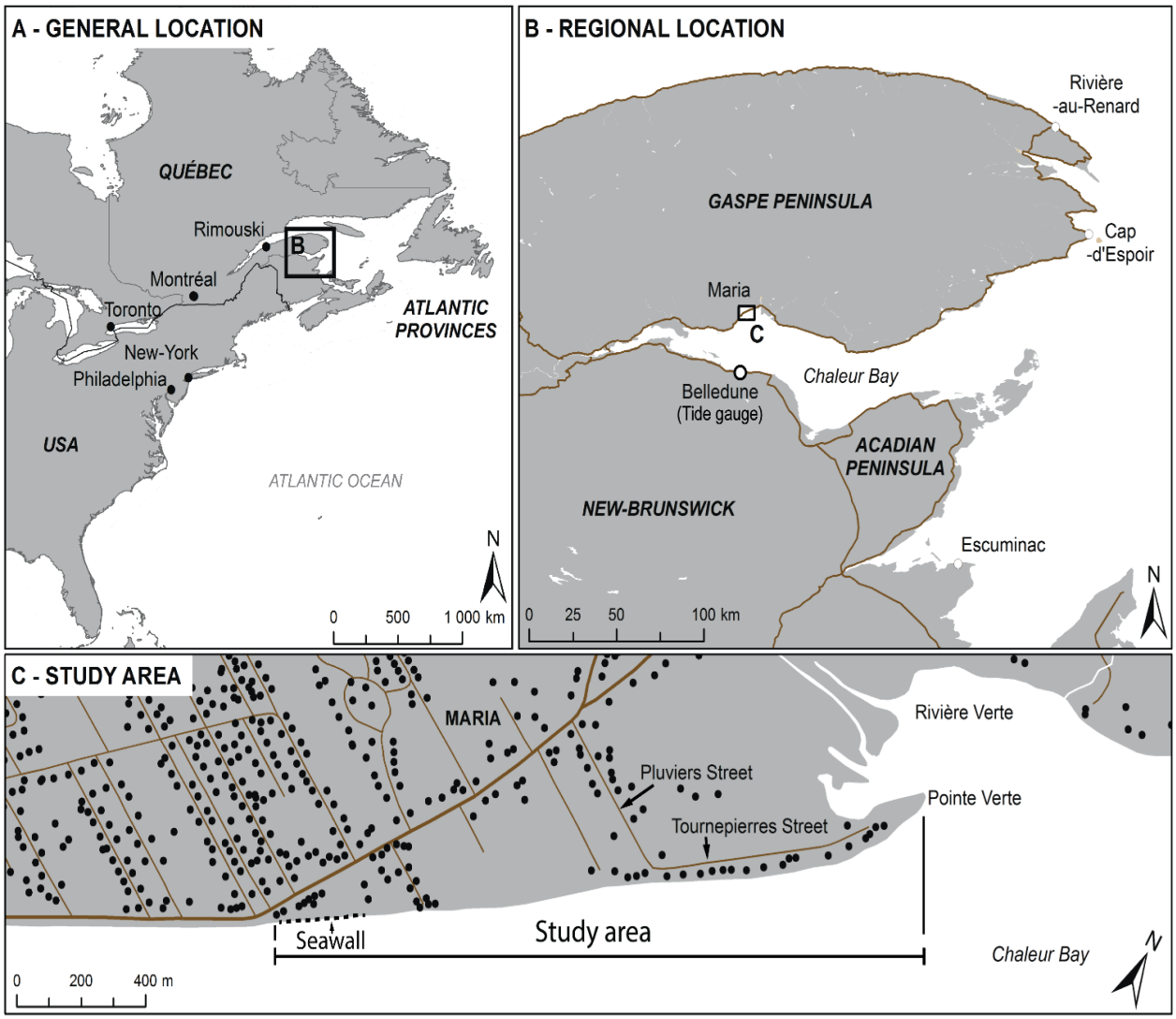

Figure 1. Location map of the study area in Maria (Quebec) on the north shore of the Chaleur Bay.

At the western zone of the study site, almost the entire beach has been eroded as a result of wave reflection and scouring at the wall toe [51,52] (Figure 2b). Beach erosion has exposed a substrate of pebbles and gravel (Figure 2b). Backshore elevation in this area is higher than in the eastern part of the site. The region experiences a semi-diurnal and meso-tidal regime, with a mean sea level (MSL) of 1.33 m relative to Chart Datum [76] (Table 1). During highest astronomical tide (HAT) (1.66 m), the seawall toe is submerged and oscillating water levels occur on the seaward face of the wall. As observed during the 2005 flood event [52], continuous wave overtopping can occur during periods of high water levels and large waves.

Figure 2. The beach of the study area is mainly natural on the eastern part (**a**) and characterized by a seawall on the western coastline (**b**).

Table 1. Mean estimated tidal values in 2010 according to chart and geodetic datum, Belledune station (NB) (Canadian Hydrographic Service).

Water Levels	Mean Estimated Value (2010) Chart Datum (CD)	Canadian Geodetic Vertical Datum 1928 (CGVD28)
Extreme level (tide + storm surge)	3.64	2.46
Highest Astronomical Tide (HAT)	2.84	1.66
Mean Sea Level (MSL)	1.33	0.15
Lowest Astronomical tide (LAT)	0.1	−1.08

3. Methodology

3.1. Post-Storm Surveys

Storm debris [77,78] and tidal deposits [79] can be used as water level limit and maximum runup extent indicators. A field survey was conducted on the day of, and immediately following, the 6 December 2010 flood event, in order to identify maximum flood water levels reached at Maria (Figure 3a).

Storm debris lines were located *in situ* using a DGPS Thales ProMark3 system (Figure 3b), with horizontal (x, y) and vertical (z) uncertainties of ± 1 cm. A total of 188 data points were collected for the 2010 event along debris lines, which were located along 2.2 km of coastline. A database of georeferenced points was then superimposed over a 2007 airborne LiDAR raster elevation data map (spatial resolution of 1 m, vertical accuracy of 20 cm) in ArcMAP. The points were connected together to form a continuous line indicating the landward limits of the water during the storm. Points were then generated every 5 m along the line and elevation values were extracted from the raster providing mean flood elevations for the (protected) western and (unprotected) eastern zones, relative to geodetic datum CGVD28.

3.2. Mobile Terrestrial LiDAR Data Acquisition

The alongshore and cross-shore variability in beach morphology at Maria has been studied by Bernatchez *et al.* [52] using DGPS profiles. Even if the natural beach is mainly homogenous in terms of sediments and morphological patterns (width, volume), morphological variability exists between areas with defense structures (west zone) and those in a quasi-natural state (east zone). We initially used

airborne LiDAR data to map the first coastal defense line, but the spatial resolution and accuracy in *z* does not allow us to determine with sufficient precision the height of the crest elevation. We therefore used mobile terrestrial LiDAR system (MTLS) on the entire beach of the study area on 28 September 2011 (Figure 4a) to improve on spatial resolution and vertical precision of previous studies [51,52]. The survey was conducted at low tide and covered the entire foreshore to a minimum seaward elevation of 1 m below CGVD28 (close to LAT).

Figure 3. Field survey after the flood showing (**a**) flood generated overwash fan and (**b**) the debris line delineation. Limits were located using DGPS on the day following the storm event (Maria, 7 December 2010).

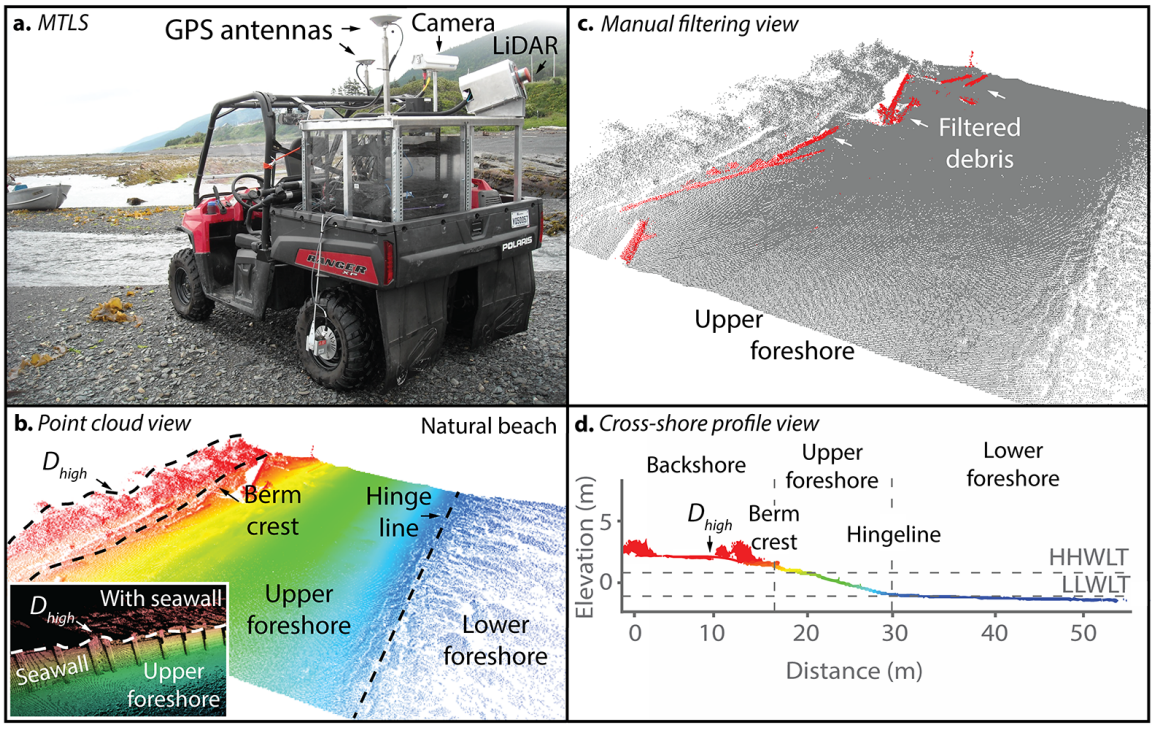

Figure 4. Mobile terrestrial LiDAR system (**a**) with point cloud and filtering view examples (**b**,**c**). Resulting data are used in cross-shore view to localize the first ridge on the natural beach or the coastal structure crest elevation (D_{high}), the berm crest and the hinge line (**d**).

The MTLS is a multi-sensor system mounted on a utility side by side vehicle (Figure 4). The multi-sensor system includes a laser scanner Riegl VQ-250, a camera PointGrey Grasshopper GRAS-50S5C-C and a GPS inertial navigation system Applanix POS-LV 220 (Figure 4a) [80]. Post-processing was performed using PosPAC and Trimble Trident Analyst software. The projection used was NAD83 MTM5 with geoid HT2.0. The LiDAR point cloud has a spatial resolution of less than 0.05 m × 0.05 m (Figure 4b). Different types of beach debris were filtered manually in LP360-QCoherent software (Figure 4c). A grid elevation with a spatial resolution of 0.5 m was created in LP360-QCoherent software in order to identify the beach slope with high accuracy.

The first line of defense (D_{high}), corresponding to the defense structure crest in the west zone, or to the crest elevation of the first ridge landward of the berm crest in the east zone, was manually digitized in ArcMAP. To calculate the accuracy of the laser data, a total of 23 control points were measured using a D-GPS Trimble R8 over the entire study site. The error was calculated by the root-mean-square (RMS) of the difference between control points and the adjacent laser points. Calculated horizontal (x,y) and vertical (z) errors are ± 0.03 m (RMS).

3.3. Hydrodynamic Data Analysis

3.3.1. Wave Dataset

No measured wave data are available for the Chaleur Bay. We therefore used a modelled wave dataset from Environment Canada's (EC) operational wave forecasting model based on WAM cycle 4 MW3 "PROMISE" [81–84]. Archived outputs cover a 10-year period, from 1 January 2003 to 31 December 2013 with a data hiatus for 2006. Time series are available at three-hour increments.

EC's implementation of WAM extends throughout the St. Lawrence Gulf and Estuary, from Montmagny to Cabot Strait and Belle-Isle Strait, at a spatial grid resolution of 0.04° latitude and 0.06° longitude (approximatively 5 by 5 km at 45° north). Selected source terms include formulation for exponential wave growth [85], formulation for linear wave generation [86], formulations for deep and intermediate water non-linear wave–wave interactions (quadruplets) and dissipation due to whitecapping [81], JONSWAP formulation for dissipation due to bottom friction [87], and formulation for dissipation due to depth-induced breaking [88].

Wave propagation schemes include refraction over bottom and non-stationary ambient currents. Non-stationary boundary conditions are based on 40 m tri-hourly winds from EC's Global Environmental Multiscale Model (GEM) and surface currents (at 5 m depth) from EC's oceanographic model of the Estuary and Gulf of St. Lawrence (MOR). Output wave parameters derived from spectra are significant spectral wave height (H_{m0}), mean spectral wave period (T_{m02}) and mean wave direction (*Dir*).Wave data quality has been assessed by Jacob *et al.* [84] and Lambert *et al*. [89–91] for the Estuary and Gulf of St. Lawrence domain. Selected data for this study were extracted from EC's model at grid point i = 67, j = 69 (−65.950 O, 48.1 N), located 7 km east south-eastward from Maria's shoreline, to a depth of −18.2 m. Given the limited fetch length in front of Maria (70 km), most simulated wave periods were under 5 s. We therefore selected a position for wave parameter extraction close to the shore yet remaining in deep-water conditions ($d >$ 1/2 L_0) for most wave periods. Selected wave records were

linearly interpolated to an hourly resolution in order to match temporal resolution with the available tidal dataset.

3.3.2. Determination of Near-Shore Wave Parameters

Runup values, as a result of wave setup and uprush, are determined by deep-water significant wave conditions (H_0 and L_0) and beach slope with the Stockdon *et al.* equation [29]. Wave shoaling and refraction over coastal waters can be empirically determined using weighting coefficients rather than physical computations. We will refer to H_0 in the paper as a reference to H_{m0}. The depth of wave breaking and the location of the break point on the sloping beach or relatively to a defense structure is an important factor contributing to erosion and flooding. Depth of breaking d_b is computed from (1) [92]:

$$d_b = \frac{1}{g^{1/5}\gamma^{4/5}}\left(\frac{H_0^2 C_0 \cos\theta_0}{2}\right)^{2/5} \quad (1)$$

where γ = 0.8, θ_0= deep-water wave angle relative to shore normal direction (incident wave = 0°), and deep-water phase velocity $C_0 = \frac{gT}{2\pi}$.

3.4. Wave Runup Estimation and Coastal Morphology

The flood assessment applied in this paper estimates wave runup with the empirical formulation proposed by Stockdon *et al.* [29] based on *in situ* measured runup values via extensive research conducted on ten sandy field experiments in the USA and Netherlands. The following equation has been applied because it is valid for a broad range of reflective to dissipative beaches:

$$R_{2\%} = 1.1\left(0.35\tan\beta(H_0L_0)^{1/2} + \frac{[H_0L_0(0.563\tan\beta^2 + 0.004)]^{1/2}}{2}\right) \quad (2)$$

where $R_{2\%}$ is the elevation above the still water level that is exceeded by 2% of the wave runups [53] and $\tan\beta$ is the beach slope. This empirical runup formulation (RMS error = 0.38 m), hereinafter referred to as the RS06 model, is considered a good predictor of runup [25,33,93] and is often used in coastal flood and vulnerability assessment [67,94–96]. The static flood model applied in this paper consists of a summation of observed tidal level and storm surge, wave characteristics and wave runup according to the RS06 empirical model. It is based on the comparison of total water level (TWL) against ground elevation assuming an instant and constant flood surface on the area [67]. Despite its simplicity, the RS06 formulation requires a beach morphology assessment. In natural settings, the beach slope is not a straightforward calculation [32,39,97]. Some authors suggest using the foreshore beach slope in the computation of the empirical formula [29,30,63,96]. Cariolet and Suanez [32] obtained a good fit relationship between measured and predicted runup using the slope of the active section of the beach in a macrotidal environment, which corresponds to the upper foreshore slope. This is in accordance with Stockdon *et al.* [25] who used the mean beach slope between the berm crest and mean high water level to define $\tan\beta$ in storm conditions where the swash is moved up the beach. Two beach slopes on the natural beach were compared in our approach (Figure 5).

Beach slope at high tide during the flood event corresponded to the slope between the point of maximum runup elevation on the beach (R_{max}) and $T_{obs} - 1.5H_0$ [43], where T_{obs} is the still water level

without the wave component. This slope, referred to as $\tan\beta_{1.5H0}$, was compared to the upper foreshore slope ($\tan\beta_{ufs}$). The upper foreshore slope is relatively located upward of mean sea level (CGVD = 0.15 m) and is located between the point of maximum runup elevation and the hinge line. Considering the maximum flood height along the coast on 6 December 2010, R_{max} is assumed to be equal to the berm crest elevation in both situations. Both berm crest and hinge line were manually delineated for the entire beach as a line feature in LP360 using a 3D visualization window (Figure 4b,d). The width of the beach Y_1 was calculated between beach berm crest and $T_{obs}-1.5H_0$. Using the MTLS derived raster, a contour line equal to $T_{obs}-1.5H_0$ was automatically digitised in ArcMAP. The mean beach slope, $\tan\beta_{1.5H0}$, was then defined $(Z_{crest}-Z_{Tobs-1.5H0})/Y_1$. The mean beach slope, $\tan\beta_{ufs}$, given a beach width Y_2 between the berm crest and the hinge line, equals to $(Z_{crest}-Z_{Hinge\ line}/Y_2)$. Beach slopes were calculated every 50 meters along the coast, for a total of 28 cross-shore profiles.

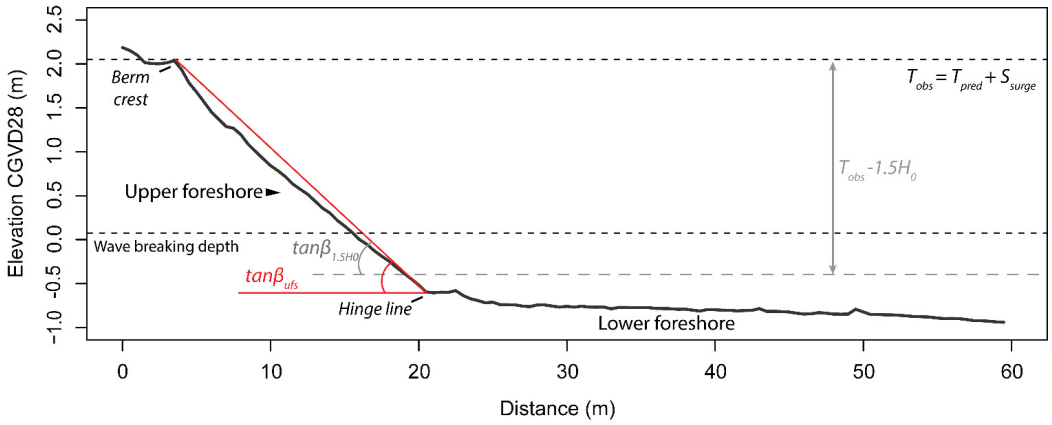

Figure 5. Natural beach slopes definitions used in the empirical runup formula. The slope $\tan\beta_{1.5H0}$ is located between the point of maximum runup elevation on the beach (R_{max}) and $T_{obs}-1.5H_0$. The upper foreshore slope ($\tan\beta_{ufs}$) is located between the point of maximum runup elevation and the hinge line. See the profile location in Figure 10, on the beach only (black line).

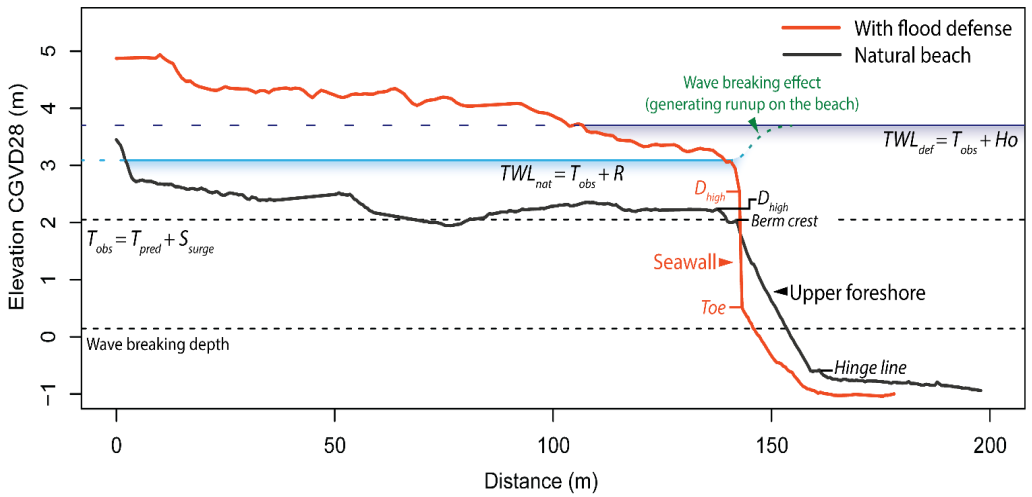

Figure 6. Sketch of the morphological difference between the defended (red) and natural (black) coastline. Modelled TWL are shown for both the natural beach (light blue) and defended coastline (dark blue). Profile locations are shown in Figure 10.

In the present study, where high water levels and wave conditions led to overtopping and flooding, bottom induced wave breaking was located close to the seawall. Since radiation stress induced wave set-down is at its maximum at the breaking point and static wave setup starts at the breaking point [98], we can assume that there is no contribution of wave setup to the total water level on the wall. As a consequence, neither runup nor setup were calculated in front of the seawall in the west zone. During the 6 December event, the cumulative offshore wave height plus storm water level elevation overtopped the defense crest by several tens centimeters. Thus, an approach using only the wave height as a criterion for flood assessment has been proposed (Figure 6).

3.5. Sea-Level Rise Projection and Flood Mapping

3.5.1. Sea-Level Analysis

Relative sea-level rise, as a result of regional glacio-isostatic adjustment and eustatic contributions, is a concern along Atlantic Canada in terms of future coastal flood risk assessment [59,63,71,99]. In the southern Gulf of St. Lawrence, the isostatic crustal movement ranges from −1 to −4 mm/year [22,23]. In Maria, the rate is estimated to be −1.78 mm/year) [100]. The nearby tide gauge at Belledune (Figure 1) provides a local relative sea-level trend of 4.06 mm/year between 1964 and 2014 for the study site, which is located 36 km northwest of the tide gauge. This tide gauge recorded data in 1964 and between 2000 and 2014. Hourly observed water levels were imported from the Canadian Tides and Water Levels Data Archives, available online [101]. The hourly predicted water levels were provided by the Canadian Hydrographic Service and were used to calculate the magnitude of surges [102]. Original tidal data are expressed relative to Chart Datum, which is 1.18 m below geodetic datum (CGVD28). All tidal and elevation references are expressed relative to CGVD28. Hourly data were smoothed to obtain monthly mean tidal levels from which the sea-level rise (SLR) trend was extrapolated. The averaged seasonal cycle and months containing less than 90% of data were removed following Daigle [103]. The SLR trend was obtained using linear regression following [104]:

$$Y = b_0 + b_1 X + \varepsilon \quad (3)$$

where b_1 is the regression coefficient estimating the SLR trend. An estimation of future water levels with the associated confidence intervals was also performed following the approach by Boon [104].

3.5.2. Estimation of Return Periods for Extreme Water Levels

For the natural beach at Pointe Verte, hourly wave runup time series were combined with measured sea-level (T_{pred} + surge) providing total water level (TWL_{nat}), following Ruggiero *et al*. [34]. For coastal flooding assessment, extreme water levels are most relevant. Different approaches based on observed water levels exist to calculated return periods [65,105–107] but all of them except the peak over threshold model [106] are time-series length dependent. Since the joint times series of wave runup data and water level data is relatively short (eight years), the peak over threshold model with the generalized Pareto distribution was used to compute return periods associated with extreme water levels [106]. This method is widely used elsewhere in the northern Atlantic for extreme water level predictions [108–110]. The analysis was performed on daily maximum levels (high water tide + sea level rise + surge + wave runup)

rather than hourly values to avoid temporal dependence. A flood map assessment was performed for the 2010 event based on identified field debris and the RS06 model. The associated return period of this event was calculated with the Pareto analysis. Considering the relatively short time series of tidal data available from Belledune station, we limit the time horizon for flood mapping to 2030. Adding the sea level projection to tidal, barometric surge and runup components gives a future scenario of the same return period for any given year. For the natural beach:

$$TWL = T_{pred} + S_{surge} + R + SLR \quad (4)$$

where SLR is the sea-level rise between 2010 (T_1) and any future year T_2. For the artificially protected area, the runup component R is replaced by H_0 (see Section 3.4) thence, for defense structures:

$$TWL = T_{pred} + S_{surge} + H_0 + SLR \quad (5)$$

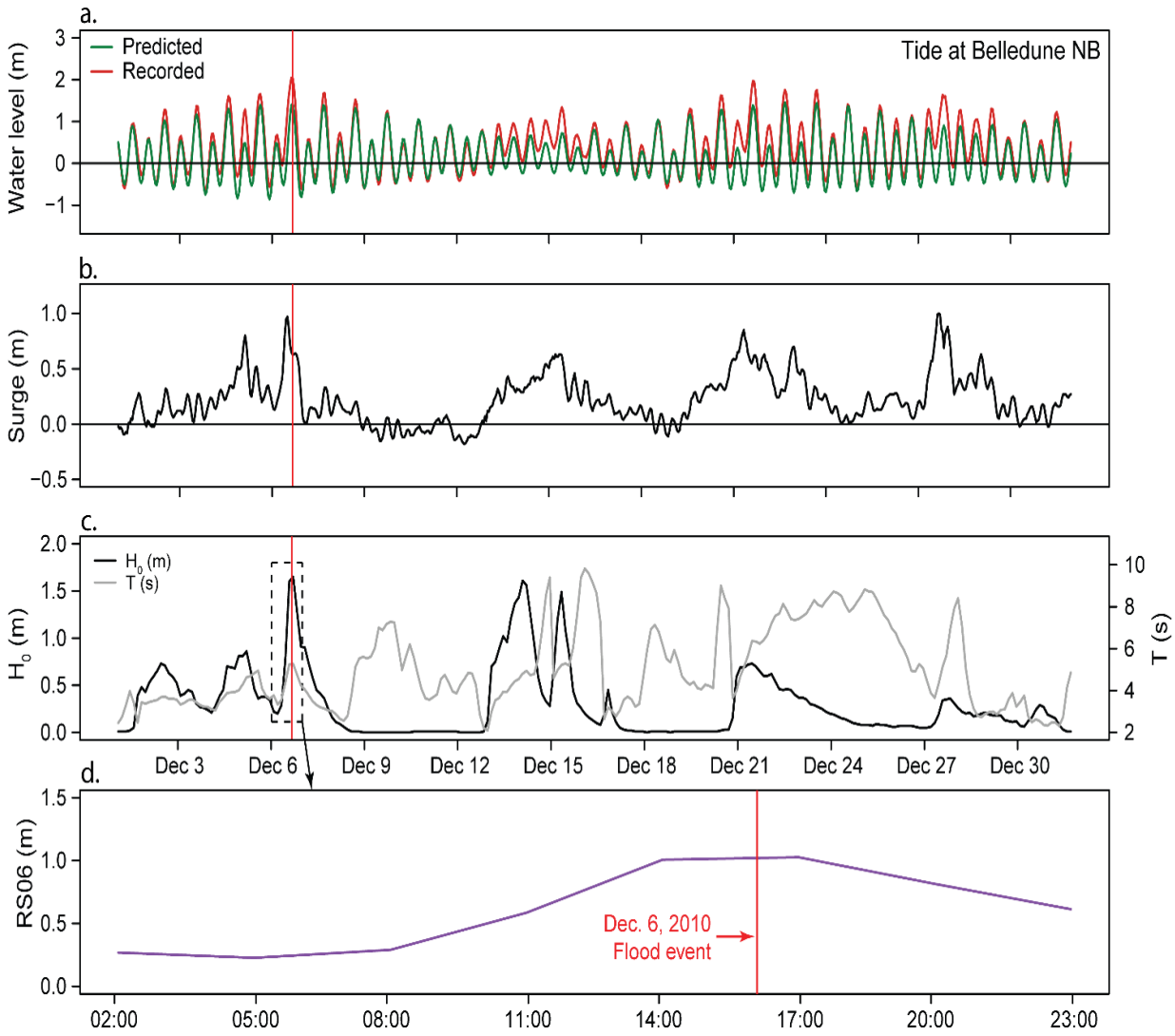

Figure 7. Tidal and hydrodynamic data on 6 December 2010. (**a**) Represents predicted and observed tide (m) at Belledune tide gauge and (**b**) The residual surge (m). The storm surge occurred during high waves reaching 1.63 m (**c**). (**c,d**) show the flooding event on 6 December, where a 1.02 m wave runup was estimated at 4:00 p.m. local time (8:00 p.m. UTC).

4. Results

4.1. Coastal Flood Mapping for the 6 December Event

4.1.1. Flood Event Analysis

During the day of 6 December 2010, the Belledune tide station recorded a high water level of 2.05 m at 4:00 p.m. local time (20:00 p.m. UTC), which included a storm surge of 0.63 m combined with an astronomical tide of 1.42 m (Figure 7a,b). Despite the fact that this water level was below the beach crest along most of the coastline (Figure 8), a significant area of the municipality of Maria was flooded by extreme water levels (Figure 9).

Mean observed flood limits reached 3.68 m and 3.07 m for areas with and without defense structures, respectively, therefore exceeding the observed tidal level (T_{obs}) by 1.63 m. The vertical seawall in the west zone increased total water elevations along this part of the coastline by 0.61 m in comparison to the natural zone. This is at least partly a result of the proximity of the wall to the still water level. The wall faces frequent wave impacts during such tidal conditions and the wall toe is completely submerged by more than 1.7 m of water depth, regardless of the wave component. Focusing on the wave breaking depth (D_b) enables a better understanding of the wave-breaking pattern both near the wall and on the natural beach (Figure 6). According to Equation (1), D_b = 1.96 m, providing a geodetic elevation of 0.09 m. Waves therefore break close to the toe of the wall, whilst in natural areas, breaking occurs on the foreshore slope (Figure 6). Where the seawall is built, no wave runup occurs. Instead, waves reach the defense almost at the breaking point.

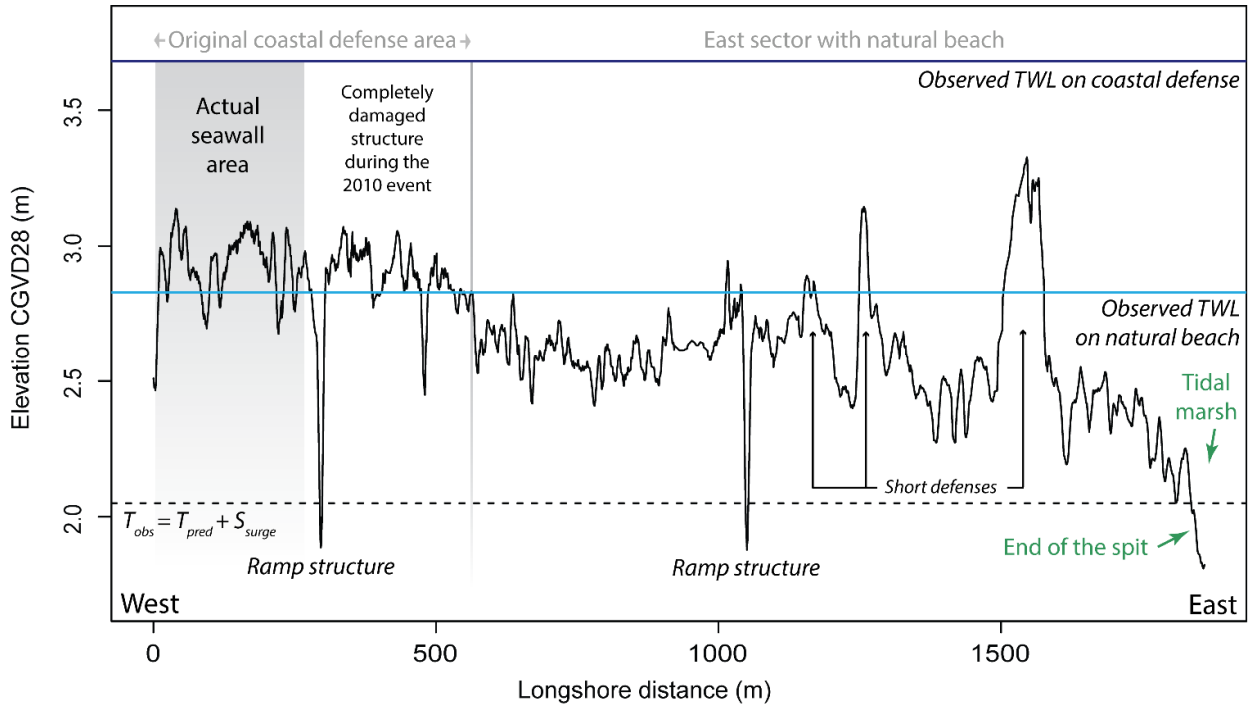

Figure 8. Recorded tide level (dashed black line) and mean observed flood limits along the coast. Longshore coastline crest elevation (D_{high}) variability between the natural zone and areas with defense structures (solid black line). Observed total water levels for the defended zone (dark blue line) exceeded those for the natural areas (light blue line).

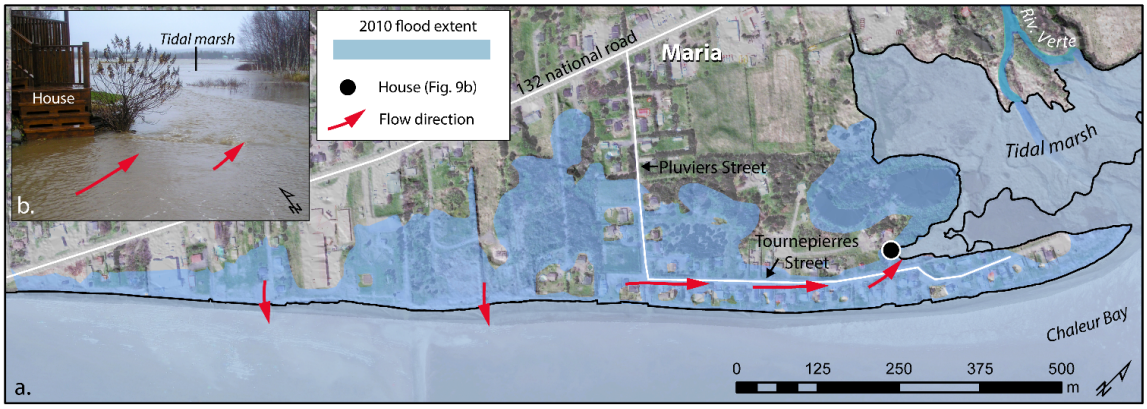

Figure 9. (**a**) Flood extent as identified during the post-storm survey and location of the flow directions in response to land drainage; (**b**) The east zone, the landward side of the spit base acts as a natural outlet for the incoming drained seawater toward the tidal marsh. The picture was taken at 3:00 p.m. (local time) on 6 December, one hour before the flood peak.

During the 6 December 2010 event, unidirectional and landward flow submerged 0.18 km^2 of the coastline at Maria. Overwashed sediments were observed (see Figure 3a) to extend up to 20 m landward in the east and 30 m landward in the central part of the study site. Following north-westward landward propagation, flood waters receded in the opposite direction following land slope, drainage channels and pipes. Much of the floodwater drained along Tournepierres Street and through the tidal marsh (Figure 9b). As a result of this eastwards drainage via the tidal marsh, the landward flow of water in this zone was limited (Figure 9a). Houses located on embankments landwards of short defense structures (Figure 8) were spared from flooding. Results show that, despite the observed tide not reaching the beach or the defense crest on 6 December 2010, heavy flooding occurred along the entire Pointe Verte coastline in Maria due to wave effects. In the western zone, almost half of the original wooden seawall was destroyed during the event, probably due to different material robustness along the defense structure (see Figure 8). Where the wall material was older and thus the protection less sturdy, much of the beach was returned to a natural state in front of many properties.

4.1.2. Wave Runup Implications in Modelling Total Water Level for Flood Mapping

Calculated beach slopes show minimal variability and have a mean value of 0.14, with a mean standard deviation of 0.013 for $\tan\beta_{ufs}$ and 0.017 for $\tan\beta_{1.5Ho}$. We considered this mean value representative of the study area and valid for the cross-shore transect approach assuming an inshore wave direction perpendicular to the shoreline. The linear regression between the upper foreshore beach slope and the slope located between the berm crest and T_{obs}-$1.5H_0$ shows a good correlation ($r^2 = 0.87$, p-value < 0.001). Therefore, the upper foreshore beach slope was used in the RS06 formulation associated with the 2010 event.

The RS06 modelled runup (Figure 7d) and TWL for the natural beach was 1.02 m and 3.07 m, respectively. Observed total water level on the natural beach was 2.83 m (Table 2), thus resulting in a coastal inundation throughout Pointe Verte. The RS06 model predicts TWL to within uncertainty ranges (RMS = 0.38 m) of the RS06. Considering the relatively constant coastline elevation (D_{high}) (2.66 ± 0.28 m standard deviation), observed tidal levels fail to overtop the coastline crest (D_{high}) without the influence

of wave effects. Wave breaking effects transfer wave energy into potential energy in the form of wave runup and thus create the potential for flooding to occur. Along the coastal defense, however, results show a higher observed TWL by at least 0.86 m compared to the natural beach (Figure 6 and Table 2), giving a water level of 3.69 m. With a 0.01 m underestimation difference, the estimated TWL on coastal defense gives 3.68 m, suggesting that adding the wave height to the still water level is a good approach to predict TWL in this case.

Table 2. Flood characteristics according to observed and predicted total water levels along natural and defended areas during the 2010 event.

2010 flood characteristics		
Coastline state	Natural beach	Coastal defense
Wave components (m)	Runup	H_0
	1.02	1.63
Time (UTC)	20:00	
Predicted tide	1.42	
Observed tide + Surge	2.05	
Surge only	0.63	
Estimated TWL (m)	3.07	3.68
Mean observed TWL (m) (*post-storm survey*)	2.83	3.69
	Estimated flood area (km^2)	Observed flood area (km^2)
Entire study area	0.267	0.179
West of Pluviers Street only	0.096	0.092
East of Pluviers Street only	0.171	0.087
West area with coastal structure	0.005	0.006

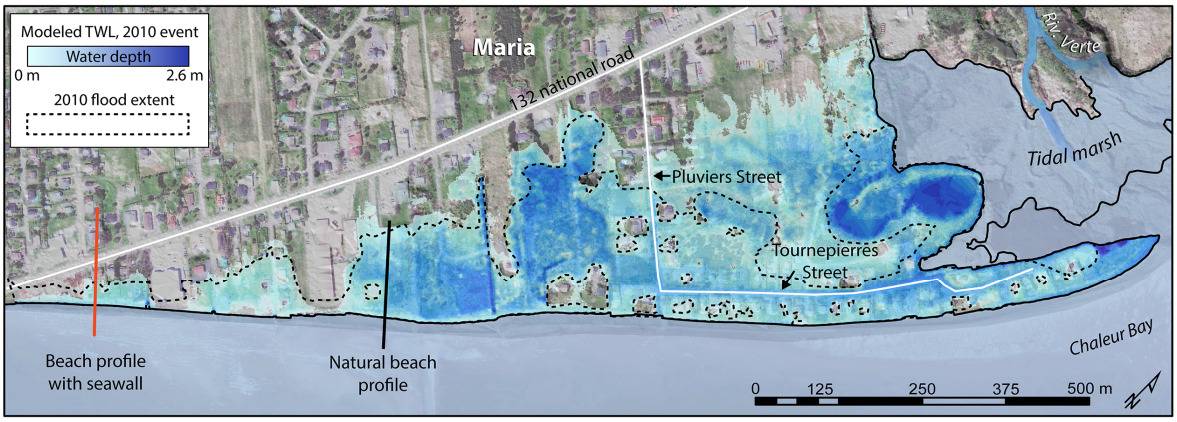

Figure 10. Modelled total water levels for the 2010 flood extent. The dashed line represents the observed flood extent during the post-storm survey. Red and black lines show profiles illustrated in Figure 6.

Estimated total water levels obtained from Equations (4) and (5) for the 2010 event were mapped over the 2007 LiDAR grid elevation whilst the data from the mobile terrestrial LiDAR system were used for defining crest elevations (D_{high}) (Figure 8). For the west and east areas, the predicted TWL estimates

well the flooded surface. The static approach, however, does not take into account the flow pattern landward of the spit and therefore overestimates the overall flood extent by 0.088 km^2 (Table 2). The overestimation is mainly attributed to the area eastward of Pluviers Street, where the model overestimates TWL by 0.084 km^2. Considering westward of Pluviers Street, modelled and measured flooded surfaces are strongly correlated with a difference of only 0.004 km^2. The area protected by the seawall also offers good correlation between both surfaces where only 0.001 km^2 is underpredicted by the model. The static approach thus represents well the flood extent when a landward driven flow occurs compared with a drained area. The results also show that Environment Canada's (EC) operational wave forecasting model based on WAM cycle 4 MW3 "PROMISE" produced reliable data for the mapping of coastal flooding at Maria. This model was used for the first time to validate coastal flooding mapping applications.

4.2. Tidal Analysis and Sea-Level Trend

According to the Belledune tide station, the measured relative SLR trend was 4.06 mm/year between 1964 and 2014 (Figure 11). Once modelled with the peak over threshold method with a generalized Pareto distribution, the estimated total water level (including tides, surge and wave runup estimations) during the 6 December 2010 event exceeded the 100 years return period (Figure 12a) and corresponds to a level of 3.01 ± 0.78 m in 2010 and 3.09 ± 0.78 m in 2030. The observed water level on the natural beach (2.83 m) did not exceed the modelled water level and corresponds to a return period of 46 years. In the zone with vertical defense structures, the total water level (including tides, surge and deep-water significant wave height) reached 3.69 m during the 6 December 2010 event. This value has an annual probability of 0.0005 (Figure 12b).

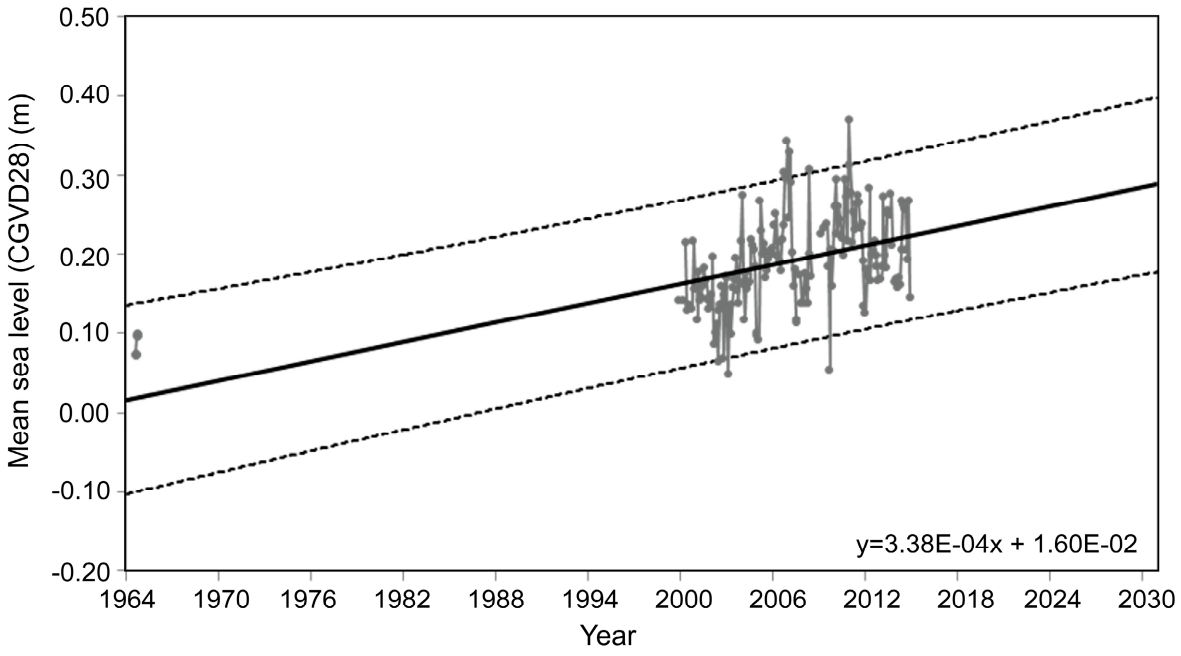

Figure 11. Linear model (solid line) fitted to 1964–2014 monthly mean sea levels at Belledune with 95% confidence bands. Linear term is statistically significant (99%).

Return periods (Figure 12) are particularly high considering only eight years of data are available. The confidence intervals suggest that, for the natural beach, the level reached during the December 2010 event could have a return period from 30 to over 200 years. An analysis of the extreme water levels return periods for the December 2010 event was conducted in the St. Lawrence maritime estuary from the longest available time series (1897–2010) at Pointe-au-Père-Rimouski station and indicates a return period of 150 years [75], which is closer to our upper interval.

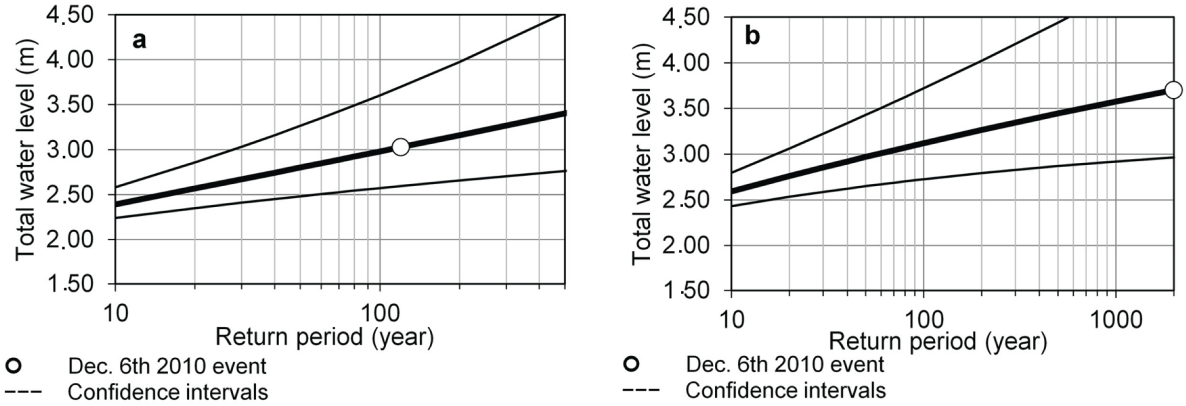

Figure 12. Estimated total water levels return periods at Belledune tide station according to the peak over threshold method including (**a**) wave runup for the natural beach on the eastern part of the study site and (**b**) significant wave height for the defended area on the west zone.

Table 3. Estimated extreme total sea levels for (**a**) (high water tide + sea-level rise + storm surge + wave runup) and (**b**) (high water tide + sea-level rise + storm surge + significant wave height) for different return periods for years 2005, 2010, 2020 and 2030 at Belledune tide station.

Estimated total water levels return periods				
		(a)		
Return Period	**Level 2005**	**Level 2010**	**Level 2020**	**Level 2030**
1 year	1.78 ± 0.11	1.80 ± 0.11	1.84 ± 0.11	1.89 ± 0.11
2 years	1.95 ± 0.14	1.97 ± 0.14	2.02 ± 0.14	2.06 ± 0.15
10 years	2.36 ± 0.30	2.38 ± 0.30	2.42 ± 0.30	2.46 ± 0.30
30 years	2.63 ± 0.47	2.65 ± 0.47	2.69 ± 0.47	2.74 ± 0.47
50 years	2.76 ± 0.57	2.79 ± 0.57	2.83 ± 0.57	2.87 ± 0.57
100 years	2.94 ± 0.73	2.96 ± 0.73	3.00 ± 0.73	3.05 ± 0.73
		(b)		
Return Period	**Level 2005**	**Level 2010**	**Level 2020**	**Level 2030**
1 year	1.95 ± 0.11	1.97 ± 0.11	2.01 ± 0.11	2.05 ± 0.11
2 years	2.14 ± 0.15	2.16 ± 0.15	2.20 ± 0.15	2.24 ± 0.15
10 years	2.56 ± 0.31	2.58 ± 0.31	2.62 ± 0.31	2.66 ± 0.31
30 years	2.82 ± 0.47	2.84 ± 0.47	2.88 ± 0.48	2.92 ± 0.48
50 years	2.93 ± 0.57	2.95 ± 0.57	2.99 ± 0.57	3.03 ± 0.57
100 years	3.08 ± 0.71	3.10 ± 0.71	3.14 ± 0.71	3.18 ± 0.71

Moreover, rising sea levels are likely to cause an increase in flood events and a shortening of return periods. A hypothetical 1 in 100 year event at Maria may become a 1 in 70 year event by 2030 (Table 3). This represents a 14% increase in frequency.

5. Discussion

Based on flood limits from post-storm survey, crest elevation and beach slope determination, wave climate modelling, wave runup estimations and sea-level rise projections, the proposed static flood approach presented here has emphasized the importance of integrating the wave component into flood assessments for low-lying coasts (Figure 13). Flood levels were identified with *in situ* measurements assuming that wave runup superimposes on tidal and surge components to increase water levels. Although runup values are mainly acquired by modelling, *in situ* measurements, or video monitoring systems [111–114], they can be estimated using measurements of field deposits [32,52,55,79]. The approach proposed here is based on deep-water wave modelling, as no wave buoy data were available for the study site during the 2010 event. The modelled results show good accordance with *in situ* measurements from the field. This is despite the empirical formula failing to account for physical processes in the surf zone [111] or the time-varying morphology of the beach in response to continuously changing wave characteristics [28].

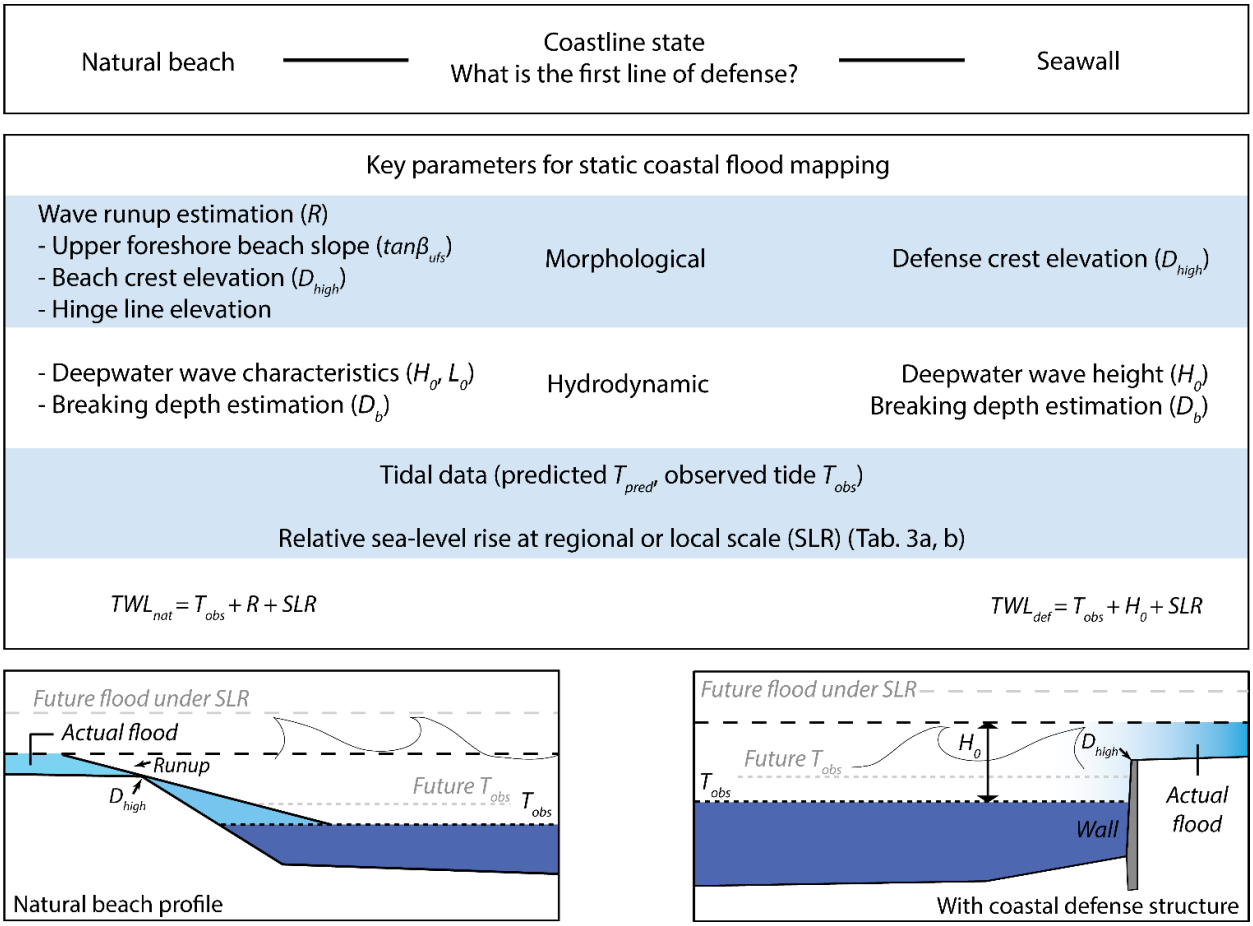

Figure 13. Conceptual and methodological approach for the static coastal flood assessment.

5.1. The Need for a Wave-Tide-Surge Integrated Approach

On 6 December 2010, no flood would have occurred in the area of Pointe Verte without a wave effect on the beach. In regards to the alongshore crest height variability and the water level observed at the tide gauge, only the concrete ramps, the end of the spit and the tidal marsh were affected by the tidal and surge components during the 2010 event. The crest elevation of both the natural beach and coastal structures was generally too high to enable a situation where the backshore would be entirely flooded by the storm surge alone [24]. Our results clearly show that the use of extreme water levels (tide + storm surge) alone, as often recommended and used for coastal flood mapping [59,61,63,64], is not necessarily sufficient for predicting coastal flooding, even in a fetch limited environment like the Chaleur Bay. The same site in 2005 experienced similar storm conditions, *i.e*. with upper foreshore limited tidal levels combined with high waves and overtopping of defense structures and overwashing of natural berms [52]. The flood extent elevation in 2005 was lower in comparison to the 2010 event (2.44 m on natural beach and 3.34 m on coastal structures), possibly due to a deep-water wave height of only 1.16 m in 2005, as obtained by the forecasting wave model in this study. Similar results have been observed on low-lying and rocky coasts of the St. Lawrence maritime estuary, where only 1% of the flooded zone between Rimouski and Sainte-Flavie would have been inundated by the tidal and surge components combined [77]. In all cases, total water levels, which caused major flooding, were increased by the wave effect. The results show the importance of integrating the wave component into the analysis of coastal flooding even for sheltered coastlines where their effects are often ignored or underestimated. Similar findings were observed in California where infrastructures at risk of flood are often concentrated around sheltered embayments. Originally, wave effects were ignored in flood analyses [58] yet subsequently have been integrated into more complete hydrodynamic flood models [67]. Other results were recently observed on the other side of the Atlantic, where in February 2010, Xynthia generated a large storm surge contributing to coastal flood in France. Bertin *et al.* [115] underlined the exceptional surface stress originating from young and steep waves propagating toward the shore, increasing water levels at coastline and contributing to flooding. For more than a decade, considering the wave component is also part of the FEMA's procedure for coastal flood mapping in the US [116–118]. Using computer programs such as Runup 2.0 and ACES (Automated Coastal Engineering System), numerical models like CSHORE, or empirical formulas, wave runup and wave overtopping are included in the flood map methodology for the National Flood Insurance Program [94].

For the natural beach of Pointe Verte, we modelled deep-water wave characteristics and integrated these into a static flood model under a wave runup empirical formulation [29]. The estimated wave implication for the 2010 event increased the still water level from 2.05 m to 3.07 m, resulting in a theoretical wave runup of 1.02 m in natural areas. This increase in water levels was also recorded by Bernatchez *et al.* [52], where an amplitude of 0.4 m over the still water level was recorded on the natural beach during the storm in December 2005.

Along the natural beach, wave runup occurs on the upper foreshore beach slope. Using this beach slope in the Stockdon runup formulation and adding this value to the observed tide and surge showed good correspondence with field debris elevation measurements. Although the foreshore slope has been used in previous works [29,32,34,67,96,119], the mean upper foreshore slope defined here was located between the beach crest and the hinge line, corresponding to the "slope of the active section of the

beach", as suggested by Cariolet and Suanez [32] for macrotidal environments. Using this beach slope, the Stockdon model showed good results in estimating wave runup and mean flood limit elevations were within model errors (±0.38 m). This is in accordance with authors who suggest using the Stockdon formula in order to estimate wave runup as a first step in coastal flood assessments [94,95]. Some studies show that the Stockdon formula tends to over-estimate the flooding extent [55,67] or occasionally underestimate it [111].

Other runup empirical formulas based on beach slope and deep-water wave characteristics exist [30,34,57,97,120] and demonstrated different results [32,77]. In our case, without precise field recordings of high frequency wave runup and near-shore hydrodynamics, we find the Stockdon model based on deep-water wave characteristics and upper foreshore beach slope suitable to our static flood model on the natural beach. The upper foreshore slope offers a practical advantage to coastal managers because it can be readily defined using GIS [51]. By digitizing the coastline and the hinge line from a series of aerial photographs and LiDAR products, one is able to estimate wave runup at high tide if wave climate data is available. This is a measureable morphological aspect that can be used in historic flood assessments and for predicting future extreme events.

As demonstrated along the seawall at Maria, wave crest elevation in relation to the height of the defense crest is also an important parameter in coastal flood management [121]. Upper foreshore sediment volumes are diminished in front of coastal structures in response to wall reflection and scouring at the toe [52,122]. Therefore, waves do not break on the foreshore until reaching the vicinity of the wall front. As a result, almost no dissipation occurs on the sloping beach in front of the wall and flood limits become higher landward of seawalls in comparison to behind natural beaches. No wave runup occurs in such cases [43] and flooding is due primarily to wave overtopping. Chini and Stansby [53] showed that the overtopping discharge was higher when beach level was lower at the toe of the seawall. This may explain the much higher TWL measured in front of defense structures compared to the natural beach in Maria. Since no wave overtopping discharge calculations were made in the present study, we propose adding significant deep-water wave heights to the still water level in order to estimate flood levels landward of the seawall. This approximation is a useful approach for coastal managers and showed good results in this study. Since coastal flood assessment and mapping for large areas can easily require time consuming and expensive studies [20], especially where complex coastal defense structures are present and require computationally demanding effort for bulk application [95], adding deep-water wave height to the observed tide (with surge) as a simple rule-of-thumb in order to obtain total water levels facing seawall can be suitable as a first approach to flood mapping in the present case where waves do not break before reaching the vicinity wall.

Another element vital to flood model robustness is the accuracy with which we can identify and map the first line of defense [25] both in natural environments and along defense structures. Recent studies show that airborne LiDAR digital elevation models, usually with a spatial resolution of 1 m and a vertical accuracy of ±15 cm [123,124] and sometimes up to 30 cm [125–127], are inadequate to determine this limit with sufficient precision as micro-scale topographic features relevant to hydraulic connectivity are overlooked [58]. The result is an over- or under-estimation of the flood extent. The mobile terrestrial LiDAR system (MTLS) that we used in this study produced a point cloud with a spatial resolution of less than 5 cm and vertical errors of ± 3 cm (RMS), which effectively solves the problem of having to determine defense crest elevation manually [25]. The MTLS also allows for much faster field surveys in

comparison to fixed terrestrial laser scanning (TLS) or DGPS, which are sometimes used in lieu of airborne LiDAR data [128]. This is an important advantage in the coastal environment as the time available to map beach morphology can be short at low tide. Surveys with the MTLS also provide potential in urban flood modelling where the representation of micro-scale topographic effects and complex features (curbs, ditches roads, defense structure crests, walls, and/or buildings) or drainage systems have significant impact on flood propagation [67,69,70]. Airborne LiDAR data covering larges areas in a rapid survey can be combined with MTLS surveys along coastal borders to maximize the advantage of both platform to generate high-resolution digital elevation models for accurate coastal flood mapping.

5.2. Inland Drainage and Sea-Level Rise

During the 6 December 2010 event, water levels in the tidal marsh at Maria were lower than the predicted flood levels due to the protection offered by the coastal spit. Marshes attenuate wave energy and provide natural resilience to flooding exposure [129,130]. Due to a land gradient landward of the coastline, however, the Stockdon model did not predict well the flood limits. This model overestimation has been reported previously when applied to other flooded peninsula environments [67] and a decelerating landward flow with distance is normally seen in this particular situation [113]. Flood limits at the tidal marsh in east Maria were below the 2.83 m average for the region. Due to the morphology of the marsh, only the astronomical tide and storm surge components affected this flooding surface during the event, demonstrating the natural protection offered by this type of environment.

The relatively low 2.05 m still water level was too low to produce an inundation regime during the 2010 event. An inundation regime occurs when a constant inland flow of water under storm surge effects (tide + surge) is realized, causing continuous submersion of the coastline [24,25]. Under future sea-level rise, conditions where the still water line is raised, an inundation regime could occur over the Pointe Verte area, which has the potential to flood the entire spit and tidal marsh. In such a case, the land drainage effect would diminish and the static flood model presented here would likely give an accurate account of flooding for the area eastward of Pluviers Street.

According to our linear SLR prediction of 4.06 mm/year (1964–2014), the return period for an equivalent storm to generate a still water level (tide + surge) reaching the beach crest of 2.66 m causing an inundation situation is 150 years. This modelled linear trend is in accordance with the IPCC's RCP8.5 sea level rise scenario for at least the next two decades.

As an example, 20 years of SLR at this constant rate produces a net rise of 0.082 m from 2010 to 2030. Integrating the IPCC's RCP8.5 sea-level scenario [131] with current isostatic land motion (−1.78 mm/year; [100]) results in a net SLR of 0.122 m by 2030, relative to 2010 levels. By integrating the IPCC's projection and Koohzare's isostatic model, we can estimate the year when an inundation regime event (at least equal to the mean coastline elevation of 2.66 m) would happen. A hypothetical 2.66 m still water level could be reached by 2081, after 71 years. Moreover, in the context of climate change, the significant reduction of sea-ice cover will promote an increase in winter storm waves hitting the coast [132].

The trend of relative SLR has been 6.96 mm/y between 2000 and 2014 at the Belledune tide gauge. This evidence of acceleration in SLR is also observed at tide gauge stations in Eastern Canada and

Northeastern United States [104]. The SLR acceleration since 1990 is a global response to the increased radiative forcing of the climate system [133]. Due to the short time series of tide gauge data, we opted for a conservative linear trend compared to the quadratic approach used by other authors to project sea-level rise [8,104].

The use of tide gauge data has the advantage of integrating both isostatic and eustatic components to project relative SLR at the regional scale [104]. However, due to the short time series and discontinuity of the tide gauge data from the Belledune station, the projection of relative SLR was made only for a short period. The recent acceleration in global SLR averages [3,4] and the large differences between scenarios of eustatic rise by 2100 [7] demonstrate the need to develop and use proxies to better establish regional relative sea-level trends [134–136]. These data will be needed to establish a more robust coastal flood risk mapping.

6. Conclusions

Wave runup estimation and modelling of water levels and deep-water waves have reproduced observed flood limit elevations during the storm event of 6 December 2010, as experienced along a natural and armoured coastline. Results clearly show the importance of integrating wave data and runup in assessing and mapping the risk of coastal flooding. They also demonstrate that the lowering of beach levels at a seawall toe increases total water level elevations in the backshore and consequently the risk of flooding due to a wave breaking occurring at the vicinity of the seawall. Our approach integrates runup, which takes into account beach slope (natural areas), or deep-water wave height (at seawalls), the return period of extreme water levels and future relative sea-level rise in order to establish, at the municipality scale, coastal flood risk maps. This approach, which takes into account several variables, is easy to use for coastal managers, which is an important factor in the process of adaptation. Such static approaches do not, however, account for land drainage. In the context of accelerating sea-level rise, it becomes necessary to establish, at the regional scale, a longer series of relative sea-level trends, a validation of wave, drainage, and numerical runup models in different geomorphological settings and hydrodynamic conditions. The next step will be to integrate wave overtopping discharge models to better represent overland flow patterns. In this perspective, the use of a mobile terrestrial laser system offers excellent potential to model and map more accurately coastal flooding. Integration of validated modelled data into a warning system offers a promising avenue for managing and mitigating coastal risks.

Acknowledgments

We thank the Quebec government for funding this project as part of its program for preventing the principal types of natural risks. Thanks as well to Tarik Toubal for the storm debris line mapping with DGPS and Susan Drejza, Patrick Bouchard and David Lacombe for the mobile terrestrial LiDAR survey. We thank Denis Jacob and Viateur Turcotte from Environment Canada for the wave data provided by the wave forecasting model, and to Phillip MacAulay (CHS) for the Belledune station data information. We also thank Azadeh Koohzare for sharing vertical crustal movement data. Thanks for the two anonymous reviewers and editors for their very pertinent and helpful comments.

Author Contributions

Field surveys (DGPS, LiDAR, flood limit): C.F., D.D., P.B., S.V.W. Hydrodynamic data analysis: D.D., A.L. Sea-level analysis: G.B.B., P.B., D.D. Flood mapping: D.D., C.F. Discussion on the results: D.D., P.B., A.L., G.B.B., C.F., R.L.B. Major contribution to the writing of the entire paper: D.D., P.B. with a main contribution of A.L. for introduction, discussion and wave analysis sections, G.B.B. for sea-level and return period for extreme water levels and S.V.W. for the methodology section of the mobile terrestrial LiDAR data. Edited English syntax: R.L.B.

Conflicts of Interest

The authors declare no conflict of interest.

References

1. Nicholls, R.J.; Tol, R.S.J. Impacts and responses to sea-level rise: A global analysis of the SRES scenarios over the twenty-first century. *Philos. Trans. A* **2006**, *364*, 1073–1095.
2. Nicholls, R.J.; Cazenave, A. Sea-level rise and its impact on coastal zones. *Science* **2010**, *328*, 1517–1520.
3. Church, J.A.; White, N.J. Sea-Level Rise from the Late 19th to the Early 21st Century. *Surv. Geophys.* **2011**, *32*, 585–602.
4. Rahmstorf, S.; Foster, G.; Cazenave, A. Comparing climate projections to observations up to 2011. *Environ. Res. Lett.* **2012**, *7*, 044035.
5. Pfeffer, W.T.; Harper, J.T.; O'Neel, S. Kinematic Constraints on Glacier Contributions to 21st-Century Sea-Level Rise. *Science* **2008**, *321*, 1340–1343.
6. Church, J.A.; Clark, P.U.; Cazenave, A.; Gregory, J.M.; Jevrejava, S.; Levermann, A.; Merrifield, M.A.; Milne, G.A.; Nerem, R.S.; Nunn, P.D.; *et al*. Sea Level Change. In *IPCC. Climate Change 2013: The Physical Science Basis*; Stocker, T.F., Qin, D., Plattner, G.K., Tignor, M., Allen, S.K., Boschung, J., Nauels, A., Xia, Y., Bex, V., Midgley, P.M., Eds.; Cambridge University Press: Cambridge, UK; New York, NY, USA, 2013.
7. Horton, B.P.; Rahmstorf, S.; Engelhart, S.E.; Kemp, A.C. Expert assessment of sea-level rise by AD 2100 and AD 2300. *Quat. Sci. Rev.* **2014**, *84*, 1–6.
8. Parris, A.; Bromirski, P.; Burkett, V.; Cayan, D.; Culver, M.; Hall, J.; Horton, R.; Knuuti, K.; Moss, R.; Obeysekera, J.; *et al*. *Global Sea Level Rise Scenarios for the US National Climate Assessment*; NOAA: Silver Spring, MD, USA, 2012.
9. Yin, J.; Schlesinger, M.E.; Stouffer, R.J. Model projections of rapid sea-level rise on the northeast coast of the United States. *Nat. Geosci.* **2009**, *462*, 262–266.
10. Howard, T.; Pardaens, A.K.; Lowe, J.A.; Ridley, J.; Hurkmans, R.T.W.L.; Bamber, J.L.; Spada, G.; Vaughan, D. Sources of 21st century regional sea level rise along the coast of North-West Europe. *Ocean Sci. Discuss*. **2013**, *10*, 2433–2459.
11. Obeysekera, J.; Park, J. Scenario-based projection of extreme sea levels. *J. Coast. Res.* **2012**, *29*, 1–7.

12. Vafeidis, A.T.; Nicholls, R.J.; Mcfadden, L.; Tol, R.S.J.; Hinkel, J.; Spencer, T.; Grashoff, P.S.; Boot, G.; Klein, R.J.T. A new global coastal database for impact and vulnerability analysis to sea-level rise. *J. Coast. Res.* **2008**, *24*, 917–924.
13. Gornitz, V.M.; Daniels, R.C.; White, T.W.; Birdwell, K.R. The Development of a Coastal Risk Assessment Database: Vulnerability to Sea-Level Rise in the U.S. Southeast. *J. Coast. Res.* **1994**, *371*, 327–338.
14. Jallow, B.P.; Toure, S.; Barrow, M.M.K.; Mathieu, A.A. Coastal zone of The Gambia and the Abidjan region in Cote d'Ivoire: Sea level rise vulnerability, response strategies, and adaptation options. *Clim. Res*. **1999**, *12*, 129–136.
15. Titus, J.G.; Richman, C. Maps of lands vulnerble to sea level rise: Modeled elevations along the US Atlantic and Gulf coasts. *Clim*. *Res*. **2001**, *18*, 205–228.
16. Solomon, S.; Qin, D.; Manning, M. *IPCC. Climate Change 2007. The Physical Science Basis*; Cambridge University Press: Cambridge, UK; New York, NY, USA, 2007.
17. Stocker, T.F.; Qin, D., Plattner, G.K.; Tignor, M.; Allen, S.K.; Boschung, J.; Nauels, A.; Xia, Y.; Bex, V.; Midgley, P.M.; *et al*. *IPCC. Climate Change 2013: The Physical Science Basis*; Cambridge University Press: Cambridge, UK; New York, NY, USA, 2013.
18. Rao, K.N.; Subraelu, P.; Rao, T.V.; Malini, B.H.; Ratheesh, R.; Bhattacharya, S.; Rajawat, A.S. Sea-level rise and coastal vulnerability: An assessment of Andhra Pradesh coast, India through remote sensing and GIS. *J. Coast. Conserv*. **2008**, *12*, 195–207.
19. Nicholls, R.J.; Hoozemans, F.M.J.; Marchand, M. Increasing flood risk and wetland losses due to global sea-level rise: Regional and global analyses. *Glob. Environ. Chang.* **1999**, *9*, S69–S87.
20. FEMA. *Atlantic Ocean and Gulf of Mexico coastal guidelines update. Final draft*; Federal Emergency Management Agency: Washington, DC, USA, 2007.
21. Walsh, K.J.E.; Betts, H.; Church, J.; Pittock, A.B.; McInnes, K.L.; Jackett, D.R.; McDougall, T.J. Using sea level rise projections for urban planning in Australia. *J. Coast. Res.* **2004**, *20*, 586–598.
22. Gehrels, W.R.; Milne, G.A.; Kirby, J.R.; Patterson, R.T.; Belknap, D.F. Late Holocene sea-level changes and isostatic crustal movements in Atlantic Canada. *Quat. Int.* **2004**, *120*, 79–89.
23. Koohzare, A.; Vaníček, P.; Santos, M. Pattern of recent vertical crustal movements in Canada. *J. Geodyn.* **2008**, *45*, 133–145.
24. Sallenger, A.H. Storm impact scale for barrier islands. *J. Coast. Res.* **2000**, *16*, 890–895.
25. Stockdon, H.F.; Sallenger, A.H.; Holman, R.A.; Howd, P.A. A simple model for the spatially-variable coastal response to hurricanes. *Mar. Geol.* **2007**, *238*, 1–20.
26. Benavente, J.; Del Río, L.; Gracia, F.J.; Martínez-del-Pozo, J.A. Coastal flooding hazard related to storms and coastal evolution in Valdelagrana spit (Cadiz Bay Natural Park, SW Spain). *Cont. Shelf Res.* **2006**, *26*, 1061–1076.
27. Soldini, L.; Antuono, M.; Brocchini, M. Numerical Modeling of the Influence of the Beach Profile on Wave Run-Up. *J. Waterw. Port Coast. Ocean Eng*. **2012**, *139*, 115.
28. Bauer, B.O.; Greenwood, B. Surf zone similarity. *Geogr. Rev.* **1988**, *78*, 137–147.
29. Stockdon, H.; Holman, R.; Howd, P.; Sallenger, A. Empirical parameterization of setup, swash, and runup. *Coast. Eng.* **2006**, *53*, 573–588.
30. Komar, P.D. *Beach processes and sedimentation,* 2nd ed.; Prentice Hall, Inglewood Cliffs: Upper Saddle River, NJ, USA, 1998.

31. Cariolet, J.M.; Suanez, S.; Meur-Férec, C.; Postec, A. Cartographie de l'aléa de submersion marine et PPR: Éléments de réflexion à partir de l'analyse de la commune de Guissény (Finistère, France). *Cybergeo* **2012**, *2012*, 1–21.
32. Cariolet, J.M.; Suanez, S. Runup estimations on a macrotidal sandy beach. *Coast. Eng.* **2013**, *74*, 11–18.
33. Ruggiero, P. Is the intensifying wave climate of the U.S. Pacific Northwest increasing flooding and erosion risk faster than sea level rise? *J. Waterw. Port Coast. Ocean Eng.* **2012**, *139*, 88–97.
34. Ruggiero, P.; Komar, P.D.; McDougal, W.G.; Marra, J.J.; Reggie, A. Wave runup, extreme water levels and the erosion of properties backing beaches. *J. Coast. Res.* **2001**, *17*, 407–419.
35. Seabloom, E.W.; Ruggiero, P.; Hacker, S.D.; Mull, J.; Zarnetske, P. Invasive grasses, climate change, and exposure to storm-wave overtopping in coastal dune ecosystems. *Glob. Chang. Biol.* **2013**, *19*, 824–832.
36. Battjes, J.A. Surf similarity. In Proceedings of the 14th International Conference on Coastal Engineering ASCE, Copenhagen, Denmark, 24–28 June 1974; pp. 466–480.
37. Cariolet, J.M. Quantification du runup sur une plage macrotidale à partir des conditions morphologiques et hydrodynamiques. *Geomorphol. Reli. Process. Environ.* **2011**, *1*, 95–108.
38. Stockdon, H.F.; Thompson, D.M.; Plant, N.G.; Long, J.W. Evaluation of wave runup predictions from numerical and parametric models. *Coast. Eng.* **2014**, *92*, 1–11.
39. Holman, R.A.; Sallenger, A.H. Setup and swash on a natural beach. *J. Geophys. Res.* **1985**, *90*, 945–953.
40. Hughes, S.A. Wave momentum flux parameter: a descriptor for nearshore waves. *Coast. Eng.* **2004**, *51*, 1067–1084.
41. Mase, H.; Asce, M.; Tamada, T.; Yasuda, T.; Hedges, T.S.; Reis, M.T. Wave runup and overtopping at seawalls built on land and in very shallow water. *J. Waterw. Port Coast. Ocean Eng.* **2013**, *139*, 346–357.
42. Na, S.J.; Do, K.D.; Suh, K.-D. Forecast of wave run-up on coastal structure using offshore wave forecast data. *Coast. Eng.* **2011**, *58*, 739–748.
43. Pullen, T.; Allsop, N.W.H.; Bruce, T.; Kirtenhaus, A.; Schüttrumpf, H.; van der Meer, J.W. *Eurotop: Wave overtopping of sea defences and related structures: assessment manual*; Environment Agency: Rotherham, UK; Expertise Netwerk Waterkeren: Utrecht, The Netherlands; Kuratorium fur Forschung im Kusteningenieurwesen: Hamburg, Germany, 2007.
44. Carbone, F.; Dutykh, D.; Dudley, J.M.; Dias, F. Extreme wave runup on a vertical cliff. *Geophys. Res. Lett.* **2013**, *40*, 3138–3143.
45. Chen, X.; Hofand, B.; Altomare, C.; Suzuki, T.; Uijttewaal, W. Forces on a vertical wall on a dike crest due to overtopping flow. *Coast. Eng.* **2015**, *95*, 94–104.
46. Peng, Z.; Zou, Q.-P. Spatial distribution of wave overtopping water behind coastal structures. *Coast. Eng*. **2011**, *58*, 489–498.
47. Van der Meer, J.W.; Verhaeghe, H.; Steendam, G.J. The new wave overtopping database for coastal structures. *Coast. Eng*. **2009**, *56*, 108–120.
48. Molines, J.; Medina, J.R. Calibration of overtopping roughness factors for concrete armor units in non-breaking conditions using the CLASH database. *Coast. Eng.* **2015**, *96*, 62–70.

49. Van Gent, M.R.A.; Van den Boogaard, H.F.P.; Pozueta, B.; Medina, J.R. Neural network modelling of wave overtopping at coastal structures. *Coast. Eng*. **2007**, *54*, 586–593.
50. Sabino, A.; Rodrigues, A.; Araujo, J.; Poseiro, P.; Reis, M.T.; Fortes, C.J. Wave overtopping analysis and early warning forecast system. In Proceedings of the ICCSA 2014, Le Havre, France, 23–26 June 2014; Murgante, B., Misra, S., Rocha, A.M.A.C., Torre, C., Rocha, J.G., Falcão, M.I., Taniar, D., Apduhan, B.O., Gervasi, O., Eds.; Springer: Cham, Switzerland, 2014.
51. Bernatchez, P.; Fraser, C. Evolution of coastal defence structures and consequences for beach width trends, Québec, Canada. *J. Coast. Res.* **2012**, *285*, 1550–1566.
52. Bernatchez, P.; Fraser, C.; Lefaivre, D.; Dugas, S. Integrating anthropogenic factors, geomorphological indicators and local knowledge in the analysis of coastal flooding and erosion hazards. *Ocean Coast. Manag.* **2011**, *54*, 621–632.
53. Chini, N.; Stansby, P.K. Coupling TOMAWAC and Eurotop for uncertainty estimation in wave overtopping predictions. In *Advances in Hydroinformatics, Springer Hydrogeology*; Gourbesville, P., Cunge, J., Caignaert, G., Eds.; Springer: Singapore, Singapore, 2014.
54. Dawson, R.J.; Dickson, M.E.; Nicholls, R.J.; Hall, J.W.; Walkden, M.J.A.; Stansby, P.K.; Mokrech, M.; Richards, J.; Zhou, J.; Milligan, J.; *et al*. Integrated analysis of risks of coastal flooding and cliff erosion under scenarios of long term change. *Clim. Chang.* **2009**, *95*, 249–288.
55. Guimarães, P.V.; Farina, L.; Toldo, E.; Diaz-Hernandez, G.; Akhmatskaya, E. Numerical simulation of extreme wave runup during storm events in Tramandaí Beach, Rio Grande do Sul, Brazil. *Coast. Eng*. **2015**, *95*, 171–180.
56. Ruggiero, P.; Holman, R.A.; Beach, R.A. Wave run-up on a high-energy dissipative beach. *J. Geophys. Res*. **2004**, *109*, 1–12.
57. Holman, R. Extreme value statistics for wave run-up on a natural beach. *Coast. Eng.* **1986**, *9*, 527–544.
58. Gallien, T.W.; Schubert, J.E.; Sanders, B.F. Predicting tidal flooding of urbanized embayments: A modeling framework and data requirements. *Coast. Eng.* **2011**, *58*, 567–577.
59. Daigle, R.J. *Sea level rise estimates for New Brunswick municipalities: Saint John, Sackville, Richibucto, Shippagan, Caraquet, Le Goulet*; The Atlantic Climate Adaptation Solutions Association: New-Brunswick, QC, Canada, 2011.
60. Perherin, C.; Roche, A. Évolution des méthodes de caractérisation des aléas littoraux. In Proceedings of the XIèmes Journées Natl. Génie Côtier-Génie Civil, Les Sables d'Olonne, France, 22–25 June 2010; pp. 609–616.
61. Richards, W.; Daigle, R. *Scenarios and Guidance for Adaptation to Climate Change and Sea Level Rise- NS and PEI Municipalities*; Atlantic Climate Adaptation Solutions Association: Halifax, NS, Canada, 2011; p. 87.
62. Prime, T.; Brown, J.M.; Plater, A.J. Physical and economic impacts of sea-level rise and low probability flooding events on coastal communities. *PLoS ONE* **2015**, *10*, e0117030.
63. Daigle, R. *Sea-Level Rise and Flooding Estimates for New Brunswick Coastal Sections*; The Atlantic Climate Adaption Solutions Association: Halifax, NS, Canada, 2012.

64. Webster, T.; McGuigan, K.; Collins, K.; MacDonald, C. Integrated river and coastal hydrodynamic flood risk mapping of the lahave river estuary and town of Bridgewater, Nova Scotia, Canada. Integrated river and coastal hydrodynamic flood risk mapping of the lahave river estuary and town of Bridgewater, Nova Scotia, Canada. *Water* **2014**, *6*, 517–546.
65. Pirazzoli, P.A.; Tomasin, A. Estimation of return periods for extreme sea levels: A simplified empirical correction of the joint probabilities method with examples from the French Atlantic coast and three ports in the southwest of the UK. *Ocean Dyn.* **2007**, *57*, 91–107.
66. Thompson, K.R.; Bernier, N.B.; Chan, P. Extreme sea levels, coastal flooding and climate change with a focus on Atlantic Canada. *Nat. Hazards* **2009**, *51*, 139–150.
67. Gallien, T.W.; Sanders, B.F.; Flick, R.E. Urban coastal flood prediction: Integrating wave overtopping, flood defenses and drainage. *Coast. Eng.* **2014**, *91*, 18–28.
68. Webster, T.L.; Forbes, D.L.; Dickie, S.; Shreenan, R. Using topographic lidar to map flood risk from storm-surge events for Charlottetown, Prince Edward Island, Canada. *Can. J. Remote Sens*. **2004**, *30*, 64–76.
69. Néelz, S.; Pender, G.; Villanueva, I.; Wilson, M.; Wright, N.G.; Bates, P.; Mason, D.; Whitlow, C. Using remotely sensed data to support flood modelling. *Water Management* **2006**, *159*, 35–43.
70. Ozdemir, H.; Sampson, C.C.; de Almeida, G.A.M.; Bates, P.D. Evaluating scale and roughness effects in urban flood modelling using terrestrial LIDAR data. *Hydrol. Earth Syst. Sci.* **2013**, *17*, 4015–4030.
71. Forbes, D.L.; Parkes, G.S.; Manson, G.K.; Ketch, L.A. Storms and shoreline retreat in the southern Gulf of St. Lawrence. *Mar. Geol.* **2004**, *210*, 169–204.
72. Masson, A.; Catto, N. Extratropical Transitions in Atlantic Canada: Impacts and Adaptive Responses. *Geophy. Res. Abstr.* **2013**, *15*, 3149.
73. Boyer-Villemaire, U.; Bernatchez, P.; Benavente, J.; Cooper, J.A.G. Quantifying community's functional awareness of coastal changes and hazards from citizen perception analysis in Canada, UK and Spain. *Ocean Coast. Manag.* **2014**, *93*, 106–120.
74. Drejza, S.; Frieseinger, S.; Bernatchez, P. Exposition des infrastructures routières de l'Est du Québec (Canada) à l'érosion et à la submersion. In Proceedings of the Actes du Colloque International Connaissance et Compréhension des Risques Côtiers: Aléas, Enjeux, Représentations, Gestion, Brest, France, 3–4 July 2014.
75. Bernatchez, P.; Boucher-Brossard, G.; Sigouin-Cantin, M. *Contribution des archives à l'étude des événements météorologiques et géomorphologiques causant des dommages aux côtes du Québec maritime et analyse des tendances, des fréquences et des temps de retour des conditions météo-marines extrêmes; Chaire de recherche en géoscience côtière, Laboratoire de dynamique et de gestion intégrée des zones côtières, Université du Québec à Rimouski*; Rapport remis au ministère de la Sécurité publique du Québec: Rimouski, QC, Canada, 2012; p. 140.
76. MacCaulay, P. Canadian Hydrographic Service, Dartmouth, N.S., Canada. Personal communication, 2015.
77. Didier, D.; Bernatchez, P.; Marie, G. *Évaluation de la submersion côtière grâce à l'estimation in situ du wave runup sur les côtes basses du Bas-Saint-Laurent, Canada (Québec)*; In Proceedings of the Actes du Colloque International Connaissance et Compréhension des Risques Côtiers: Aléas, Enjeux, Représentations, Gestion, Brest, France, 3–4 July 2014.

78. Ramana Murthy, M.V.; Reddy, N.T.; Pari, Y.; Usha, T.; Mishra, P. Mapping of seawater inundation along Nagapattinam based on field observations. *Nat. Hazards* **2012**, *60*, 161–179.
79. Cariolet, J.-M. Use of high water marks and eyewitness accounts to delineate flooded coastal areas: The case of Storm Johanna (10 March 2008) in Brittany, France. *Ocean Coast. Management* **2010**, *53*, 679–690.
80. Van-Wierts, S.; Bernatchez, P. *Relevé LiDAR terrestre à Sainte-Luce dans le secteur de l'Anse aux Coques dans le cadre d'une étude de recharge de plage en zone d'affouillement*; Chaire de recherche en géoscience côtière, Laboratoire de dynamique et de gestion intégrée des zones côtières, Université du Québec à Rimouski; Rapport remis au ministère de la Sécurité publique du Québec: Rimouski, QC, Canada, 2012; p. 29.
81. WAMDI Group. The WAM Model: A Third Generation Ocean Wave Prediction Model. *J. Phys. Oceanogr.* **1988**, *18*, 1775–1810.
82. Komen, G.J.; Cavaleri, L.; Donelan, M.; Hasselmann, K.; Hasselmann, S.; Janssen, P.A.E.M. *Dynamic and Modelling of Ocean Waves*; Cambridge University Press: New York, NY, USA; p. 556.
83. Monbaliu, J.; Hargreaves, J.C.; Carretero, J.C.; Gerritsen, H.; Flather, R. Wave modelling in the PROMISE project. *Coast. Eng.* **1999**, *37*, 379–407.
84. Jacob, D.; Perrie, W.; Toulany, B.; Saucier, F.; Lefaivre, D.; Turcotte, V. Wave model validation in the St. Lawrence river eastuary. In Proceedings of the 7th International Workshop on Wave Hindcasting and Forecasting, Banff, AB, Canada, 21–25 October 2004.
85. Janssen, P.A.E.M. Quasi-linear theory of wind–wave generation applied to wave forecasting. *J. Phys. Oceanogr.* **1991**, *21*, 1631–1642.
86. Cavaleri, L.; Rizzoli, P.M. Wind wave prediction in shallow water: Theory and applications. *J. Geophys. Res.* **1981**, *86*, 10961–10973.
87. Hasselmann, K.; Barnett, T.P.; Bouws, E.; Carlson, H.; Cartwright, D.E.; Enke, K.; Ewing, J.A.; Gienapp, H.; Hasselmann, D.E.; Kruseman, P.; *et al*. *Measurements of Wind-Wave Growth and Swell Decay During the Joint North Sea Wave Project (JONSWAP)*; Deutches Hydrographisches Institute: Delft, Netherlands, 1973.
88. Battjes. J.A.; Janssen, J.P.F.M. Energy loss and set-up due to breaking of random waves. In Proceedings of the 16th International Conference Coastal Engineering, Hamburg, Germany, 27 August–3 September 1978; pp.569–587.
89. Lambert, A.; Neumeier, U.; Jacob, D. *Évaluation du modèle WAM opéré par Environnement Canada dans le Golfe du Saint-Laurent; résultats préliminaires pour les tempêtes de l'automne 2010; Institut des sciences de la mer de Rimouski, Université du Québec à Rimouski*; Rapport technique remis au Ministère des Transports du Québec: Rimouski, QC, Canada, 2012.
90. Lambert, A.P.; Neumeier, U.; Jacob, D.; Savard, J.-P. Are regional operational wind–waves models usable to predict coastal and nearshore wave climate? In Proceedings of the 2012 AGU Fall Meeting, San Francisco, CA, USA, 3–7 December 2012.
91. Lambert, A.; Neumeier, U.; Jacob, D.; Savard, J.-P. *Évaluation du modèle WAM opéré par Environnement Canada dans le Golfe du Saint-Laurent; résultats intermédiaires pour les années 2010-2011; Institut des sciences de la mer de Rimouski, Université du Québec à Rimouski*; Rapport technique remis au Ministère des Transports du Québec: Rimouski, QC, Canada, 2013.

92. Dalrymple, R.A.; Eubanks, R.A.; Birkemeier, W.A. Wave-induced circulation in shallow basins. *J. Waterw. Ports Coast. Ocean Div*. **1977**, *103*, 117–135.
93. Matias, A.; Williams, J.J.; Masselink, G.; Ferreira, Ó. Overwash threshold for gravel barriers. *Coast. Eng.* **2012**, *63*, 48–61.
94. Melby, J.A.; Nadal-Caraballo, N.C.; Kobayashi, N. Wave runup prediction for flood mapping. *Coast. Eng. Proc.* **2012**, *33*, 1–15.
95. Kergadallan, X. *Analyse statistique des niveaux d'eau extrêmes. Environnement maritime et estuarien*; CETMEF: Margny Lès Compiègne, France, 2013; p. 179.
96. Vousdoukas, M.I.; Wziatek, D.; Almeida, L.P. Coastal vulnerability assessment based on video wave run-up observations at a mesotidal, steep-sloped beach. *Ocean Dyn*. **2011**, *62*, 123–137.
97. Nielsen, P.; Hanslow, D. J. Wave runup distributions on natural beaches. *J. Coast. Res.* **1991**, *7*, 1139–1152.
98. Dean, R.G.; Dalrymple, R.A. *Water waves mechanics for engineers and scientists. Advances Series on Ocean Engineering*; World Scientific: Singapore, Singapore, 1991; p. 368.
99. Shaw, J.; Taylor, R.B.; Solomon, S.; Christian, H.A.; Forbes, D. Potential impacts of sea-level rise on Canadian coasts. *Can. Geogr.* **1998**, *42*, 365–379.
100. Koohzare, A. University of New-Brunswick, Fredericton, NB, Canada. Personal communication, 2015.
101. Fisheries and Oceans Canada. Canadian Tides and Water Levels data Archives. Available online: http://www.isdm-gdsi.gc.ca/isdm-gdsi/twl-mne/index-eng.htm (accessed on 20 March 2015).
102. CHS–Canadian Hydrographic Service. Predicted Water Levels, numerical dataset, 2012. Available online: http://www.tides.gc.ca/eng/info/WebServicesWLD (accessed on 24 October 2012).
103. Garner, K.L.; Chang, M.Y.; Fulda, M.T.; Berlin, J.A.; Freed, R.E.; Soo-Hoo, M.M.; Revell, D.L.; Ikegami, M.; Flint, L.E.; Flint, A.L.; *et al*. Impacts of sea level rise and climate change on coastal plant species in the central California coast. *PeerJ* **2015**, *3*, e958.
104. Boon, J.D. Evidence of sea level acceleration at U.S. and Canadian tide stations, Atlantic Coast, North America. *J. Coast. Res.* **2012**, *285*, 1437–1445.
105. Gumbel, E.J. *Statistics of Extremes*; Columbia University Press: New York, NY, USA, 1958; p. 375.
106. Coles, S. *An Introduction to Statistical Modeling of Extreme Values*; Springer: London, UK, 2001.
107. Pugh, D.T.; Vassie, J.M. Extreme sea-levels from tide and surge probability. In Proceedings of the 16th on Coastal Engineering Conference, Hamburg, Germany, 27 August–3 September 1978; pp. 911–930.
108. Arns, A.; Wahl, T.; Haigh, I.D.; Jensen, J.; Pattiaratchi, C. Estimating extreme water level probabilities: A comparison of the direct methods and recommendations for best practice. *Coast. Eng.* **2013**, *81*, 51–66.
109. Petrov, V.; Guedes Soares, C.; Gotovac, H. Prediction of extreme significant wave heights using maximum entropy. *Coast. Eng.* **2013**, *74*, 1–10.
110. Tebaldi, C.; Strauss, B.H.; Zervas, C.E. Modelling sea level rise impacts on storm surges along US coasts. *Environ. Res. Lett.* **2012**, *7*, 014032.
111. Laudier, N.A.; Thornton, E.B.; MacMahan, J. Measured and modeled wave overtopping on a natural beach. *Coast. Eng.* **2011**, *58*, 815–825.
112. Holman, R.A.; Guza, R.T. Measuring run-up on a natural beach. *Coast. Eng.* **1984**, *8*, 129–140.

113. Holland, K.; Holman, R.; Sallenger, A. Estimation of overwash bore velocities using video techniques. In Proceedings of 1991 coastal sediments conference, Seattle, WA, USA, 25–27 June 1991; pp. 489–497.
114. Holman, R.; Stanley, J. The history and technical capabilities of Argus. *Coast. Eng.* **2007**, *54*, 477–491.
115. Bertin, X.; Li, K.; Roland, A.; Bidlot, J.-R. The contribution of short-waves in storm surges: Two case studies in the Bay of Biscay. *Cont. Shelf Res*. **2015**, *96*, 1–15.
116. FEMA. *Guidelines Specifications for Flood Mapping Partners, Appendix D. Guidance for Coastal Flooding Analysis and Mapping*; Federal emergency management agency: Wichita, KS, USA, 2012.
117. FEMA. *Wave Runup and Overtopping-FEMA Coastal Flood Hazard Analysis and Mapping Guidelines*; Focused Study Report for FEMA: Seattle, WA, USA, February 2005.
118. FEMA. Great Lakes Coastal Guidelines, Appendix D.3. http://greatlakescoast.org/pubs/reports /Great_Lakes_Coastal_Guidelines_Update_Jan2014.pdf (accessed on 2 June 2015).
119. Holland, K.T.; Holman, R.A. The statistical distribution of swash maxima on natural beaches. *J. Geophys. Res.* **1993**, *98*, 10271.
120. Mase, H. Random wave runup height on gentle slope. *J. Waterw. Port Coast. Ocean Eng*. **1989**, *115*, 649–661.
121. Saitoh, T.; Kobayashi, N. Wave transformation and cross-shore sediment transport on sloping beach in front of vertical wall. *J. Coast. Res.* **2012**, *280*, 354–359.
122. Sabatier, F.; Anthony, E.J.; Héquette, A.; Suanez, S.; Musereau, J.; Ruz, M.H.; Regnauld, H. Morphodynamics of beach/dune systems: Examples from the coast of France. *Géomorphol. Reli. Processes Environ.* **2009**, *1*, 3–22.
123. Jones, A.F.; Brewer, P.A.; Johnstone, E.; Macklin, M.G. High-resolution interpretative geomorphological mapping of river valley environments using airborne LiDAR data. *Earth Surf. Processes Landforms* **2007**, *32*, 1574–1592.
124. Leon, J.X.; Heuvelink, G.B.M.; Phinn, S.R. Incorporating DEM Uncertainty in Coastal Inundation Mapping. *PLoS ONE* **2014**, *9*, e108727.
125. Hodgson, M.E.; Jensen, J.R.; Schmidt, L.; Schill, S.; Davis, B. An evaluation of LIDAR- and IFSAR-derived digital elevation models in leaf-on conditions with USGS Level 1 and Level 2 DEMs. *Remote Sens. Environ*. **2003**, *84*, 295–308.
126. Aguilar, F.; Mills, J.P.; Delagado, J.; Aguilar, M.A.; Negreiros, J.G.; Pérez, J.L. Modelling vertical error in LiDAR-derived digital elevation models. *ISPRS J. Photogramm. Remote Sens*. **2010**, *65*, 103–110.
127. Han, J.; Kim, S. Spatial zonation of storm surge hazardous area in the Nakdong Estuary of Korea using high precision terrain data acquired with airborne LiDAR system and geospatial analysis. *J. Coast. Res*. **2013**, *65*, 1385–1390.
128. Schubert, J.E.; Gallien, T.W.; Majd, M.S.; Sanders, B.F. Terrestrial Laser Scanning of Anthropogenic Beach Berm Erosion and Overtopping. *J. Coast. Res*. **2015**, *299*, 47–60.
129. Arkema, K.K.; Guannel, G.; Verutes, G.; Wood, S.A.; Guerry, A.; Ruckelshaus, M.; Kareiva, P.; Lacayo, M.; Silver, J.M. Coastal habitats shield people and property from sea-level rise and storms. *Nat. Clim. Chang.* **2013**, *3*, 913–918.

130. Gedan, K.B.; Kirwan, M.L.; Wolanski, E.; Barbier, E.B.; Silliman, B.R. The present and future role of coastal wetland vegetation in protecting shorelines: Answering recent challenges to the paradigm. *Clim. Chang.* **2011**, *106*, 7–29.
131. Prather, M.; Flato, G.; Friedlingstein, P.; Jones, C.; Lamarque, J.-F.; Liao, H.; Rasch, P. Annex II: Climate System Scenario Tables. In *IPCC. Climate Change 2013: The Physical Science Basis*; Stocker, T.F., Qin, D., Plattner, G.-K., Tignor, M., Allen, S.K., Boschung, J., Nauels, A., Xia, Y., Bex, V., Midgley, P.M., Eds.; Cambridge University Press: Cambridge, UK; New York, NY, USA, 2013.
132. Senneville, S.; St-Onge Drouin, S.; Dumont, D.; Bihan-Poudec, A.-C.; Belemaalem, Z.; Corriveau, M.; Bernatchez, P.; Bélanger, S.; Tolszczuk-Leclerc, S.; Villeneuve, R. *Rapport final : Modélisation des glaces dans l'estuaire et le golfe du Saint-Laurent dans la perspective des changements climatiques*; ISMER-UQAR, Rapport final présenté au ministère des Transports du Québec: Rimouski, QC, Canada, 2014.
133. Church, J.A.; Monselesan, D.; Gregory, J.M.; Marzeion, B. Evaluating the ability of process based models to project sea-level change. *Environ. Res. Lett.* **2013**, *8*, 014051.
134. Bittermann, K.; Rahmstorf, S.; Perrette, M.; Vermeer, M. Predictability of twentieth century sea-level rise from past data. *Environ. Res. Lett.* **2013**, *8*, 014013.
135. Gehrels, W.R.; Woodworth, P.L. When did modern rates of sea-level rise start? *Glob. Planet. Chang.* **2013**, *100*, 263–277.
136. Barnett, R.L.; Gehrels, W.R.; Charman, D.J.; Saher, M.H.; Marshall, W.A. Late Holocene sea-level change in Arctic Norway. *Quat. Sci. Rev.* **2015**, *107*, 214–230.